




Article

Energy Autonomous Wireless Sensing Node Working at 5 Lux from a 4 cm² Solar Cell

Marcel Louis Meli ^{1,*}, Sebastien Favre ¹, Benjamin Maij ¹, Stefan Stajic ¹, Manuel Boebel ¹ , Philip John Poole ², Martin Schellenberg ² and Charalampos S. Kouzinopoulos ³

¹ Institute of Embedded Systems, Zurich University of Applied Sciences, 8401 Winterthur, Switzerland

² Microdul AG, 8045 Zürich, Switzerland

³ Information Technologies Institute CERTH, 570 01 Thessaloniki, Greece

* Correspondence: mema@zhaw.ch

Abstract: Harvesting energy for IoT nodes in places that are permanently poorly lit is important, as many such places exist in buildings and other locations. The need for energy-autonomous devices working in such environments has so far received little attention. This work reports the design and test results of an energy-autonomous sensor node powered solely by solar cells. The system can cold-start and run in low light conditions (in this case 20 lux and below, using white LEDs as light sources). Four solar cells of 1 cm² each are used, yielding a total active surface of 4 cm². The system includes a capacitive sensor that acts as a touch detector, a crystal-accurate real-time clock (RTC), and a Cortex-M3-compatible microcontroller integrating a Bluetooth Low Energy radio (BLE) and the necessary stack for communication. A capacitor of 100 µF is used as energy storage. A low-power comparator monitors the level of the energy storage and powers up the system. The combination of the RTC and touch sensor enables the MCU load to be powered up periodically or using an asynchronous user touch activity. First tests have shown that the system can perform the basic work of cold-starting, sensing, and transmitting frames at +0 dBm, at illuminances as low as 5 lux. Harvesting starts earlier, meaning that the potential for full function below 5 lux is present. The system has also been tested with other light sources. The comparator is a test chip developed for energy harvesting. Other elements are off-the-shelf components. The use of commercially available devices, the reduced number of parts, and the absence of complex storage elements enable a small node to be built in the future, for use in constantly or intermittently poorly lit places.

Keywords: energy harvesting; low power; solar cell; capacitive sensing; Bluetooth Low Energy; low light; power management; comparator



Citation: Meli, M.L.; Favre, S.; Maij, B.; Stajic, S.; Boebel, M.; Poole, P.J.; Schellenberg, M.; Kouzinopoulos, C.S. Energy Autonomous Wireless Sensing Node Working at 5 Lux from a 4 cm² Solar Cell. *J. Low Power Electron. Appl.* **2023**, *13*, 12. <https://doi.org/10.3390/jlpea13010012>

Academic Editors: Alessandro Bertacchini and Pierre Gasnier

Received: 3 December 2022

Revised: 22 January 2023

Accepted: 24 January 2023

Published: 1 February 2023



Copyright: © 2023 by the authors. Licensee MDPI, Basel, Switzerland. This article is an open access article distributed under the terms and conditions of the Creative Commons Attribution (CC BY) license (<https://creativecommons.org/licenses/by/4.0/>).

1. Introduction, Motivation, and Statement of the Issues

According to market intelligence, millions of IoT devices have been installed so far. Expectations are that many more will follow in the years to come. It is well understood and accepted that a large-scale deployment of Internet of Things (IoT) sensor nodes requires appropriate solutions to power the nodes and to enable reliable data transfer between the IoT devices and the gateways that convey the information to application servers [1–5]. Batteries are the established means of powering IoT nodes. However, the need to timely replace them leads to important running costs and environmental issues. The IoT nodes must be localized for battery replacement, which is not easy if they are small and if there are many of them. The frequency of such “search and replace” operations depends on the application’s energy requirements and the characteristics of the batteries. In the worst case, the nodes might not be found again and will cease operations for lack of energy. Other disadvantages of batteries are the negative impact of extreme temperatures that can seriously reduce their lifetimes and their negative environmental consequences.

Powering the nodes using energy harvested from the surroundings is an attractive alternative, and various methods have been described to achieve that purpose [1,4–9].

The harvesters might rely on temperature gradients, mechanical energy from vibrations, the presence of radio frequency fields, etc. Some examples of harvesters that convert the primary energy into electrical energy include thermoelectric generators (TEG), piezo elements, electrodynamic devices, RF antennas, and others.

This work focuses on the use of solar energy, which is one of the most efficient, promising, and popular energy harvesting methods. It works well, provided that the cells are not dirty or covered and that there is sufficient light in the operating environment. The outdoor light level is high during the day and decreases as the night sets in. Indoors, the illuminance from artificial sources varies, depending on the light level regulations for activities performed in the place of interest. In general, indoor illuminance when using artificial light sources is in the hundreds of lux. Outdoors, it is in the tens of thousands of lux. Artificial light sources are normally tailored for the visible spectrum (human eye), while natural light (from the sun) has a broader spectrum. Illuminance (lux) is therefore often used when dealing with indoor illumination. In [10], there is a list of light level recommendations for some places as follows:

- Interior parking lots, stairways and corridors: 50–100 lux.
- Classrooms and studying places in general: 300–500 lux.
- Offices in general: 300–500 lux.

These recommendations vary from country to country, and even within the same country.

Figures 1–3 show measurements of illuminances carried out in three different offices in Winterthur, Switzerland, in September 2022. Luxmeters of the type Chauvin Arnoux CA-1110 [11] were used. Light in the offices often comes from artificial sources if they are activated and from natural sources through the windows and other openings.

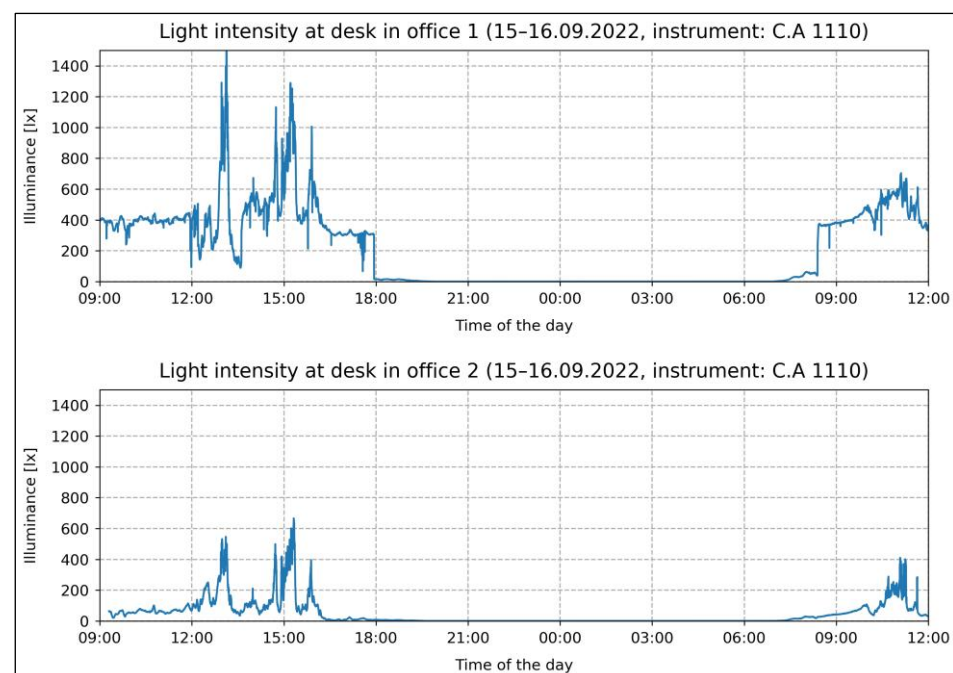


Figure 1. Illuminances on working desks in office 1 (occupied) and office 2 (unoccupied).

In the cases of Figure 1, the luxmeters were placed on work desks in office 1 and office 2, and illuminances were logged for over 24 h on a workday. Figure 2 shows a magnification of the early hours. Illuminance is affected by the time the sun rises, which depends on the time of the year. Office 2 was not occupied; therefore, the lamps were never switched on. The daylight coming through the windows was the main contributor. Office 1 was normally occupied, and lights were switched on or off during working hours as needed, leading to various contributions of daylight and artificial light. One can see

the shift in the measurements in office 1 during working hours. After work, the values suddenly sink, decrease gradually, and remain very low for many hours at night (lights switched off).

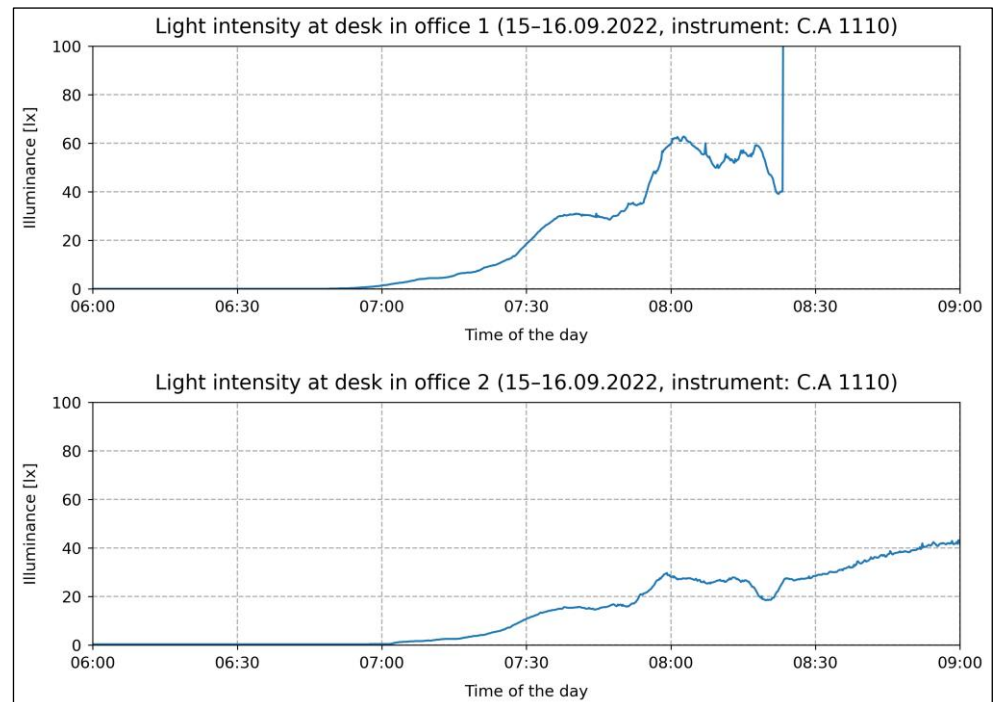


Figure 2. A closer look shows low illuminances in office 1 and office 2 early in the day.

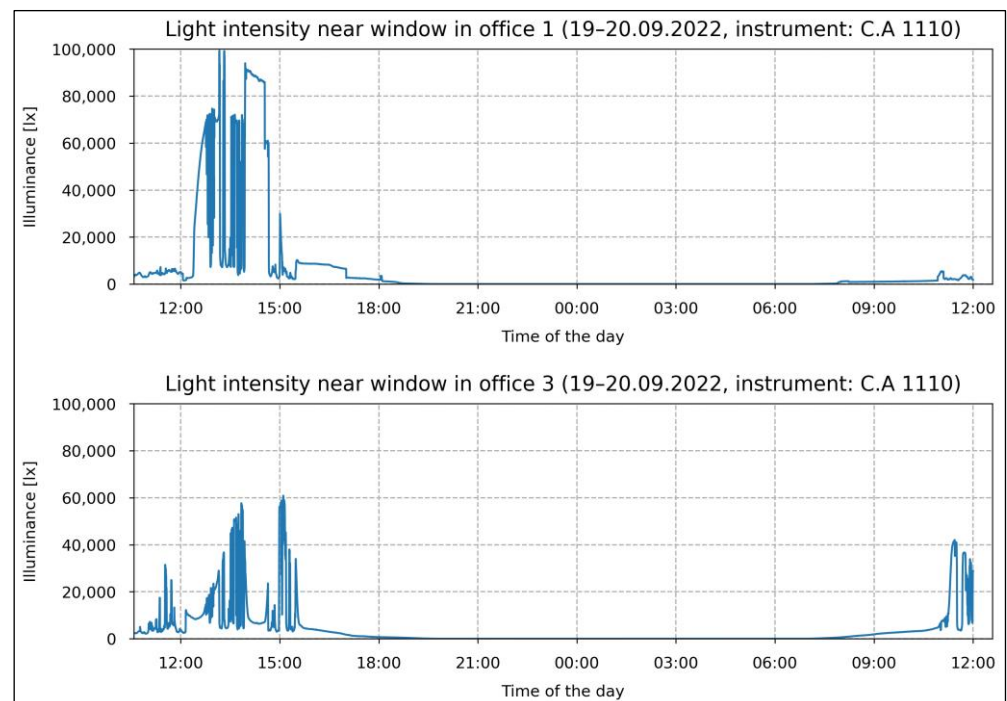


Figure 3. Illuminances in office 1 and office 3 near the windows. Luxmeters facing the window.

In the case of the results shown in Figure 3, the measurement devices were placed near a window in office 1 and in office 3. The luxmeters faced the windows, which explains the very high illuminances. Artificial light and daylight have different spectral contents, which might influence the amount of harvested energy, depending on the solar cell type. In

the case of locations exposed to both natural and artificial light, there is a mixture. Such variations are not necessarily reflected in illuminance measurements.

The measurement examples above show that it is not unusual to have places in a building or office that will stay well below 100 lux for long periods of time. The illuminance might also strongly vary during the day. Some locations might even be permanently at low light (e.g., corridors), lit only with artificial lights. For energy harvesting using solar cells, one can distinguish the following cases:

- Case 1: Places where there are periods of good illumination. Part of the harvested energy can be kept in a fitting energy storage method and used to power the system when light intensity levels are no longer sufficient. An appropriate storage management system is needed, which comes at extra cost, space, and sophistication. This is the method used in most systems. The authors of [12] provide one of the many examples that work in that way. The sophistication is partly related to characteristics such as the discharge current, the number of charge/discharge cycles, and the operational temperatures. The small number of charge/discharge cycles often contributes to shorten the lifetime of the product. However good the storage is, it will not do for spaces that are permanently under low light. This case is not the focus of this work.
- Case 2: Places that are poorly lit, either always or for so long that storing enough energy is not a viable solution. This might be the case for corridors or parking places in buildings. It is currently difficult to use solar harvesting in such places. Few works dealing with this case have been reported, as far as we know. The state-of-the-art analysis in Section 2 especially looks into works that have been found.
- Case 3: Situations where the illumination constantly varies. This happens, for instance, when dealing with portable systems powered by solar cells (such as those that can be worn). Space is very limited. The illumination on a wearable depends on how the device is worn, how it is orientated, and where it is. Solar-powered watches can be included in this category.

The AMANDA card is a wearable developed within the AMANDA project. It is a wireless sensing system powered with the help of small solar cells [13]. The device has the length and width of a credit card and can be placed on a desk or in other places in an office. It can also be worn, e.g., around the neck with an appropriate card holder (see Figure 4). The AMANDA card fits case 3 described above. Some variations of the card require only a short-range wireless system such as BLE. The embedded system on the card should periodically perform certain tasks but also asynchronously react to the user's intervention. If the card is taken out of a dark place (where it was powered off for lack of energy) and put on a table, it should quickly harvest energy and start functioning.



Figure 4. The AMANDA card can be worn, like cards on this picture.

In case 2 and case 3, it is advantageous, even necessary, to be able to scavenge enough energy under low light conditions (often described as below 200 lux). This work aims at harvesting energy in environments where the illuminance is lower than 20 lux, in order to allow continuous or intermittent sensing in such locations. The focus is on cold-starting and running under low illuminances in order to avoid the use of special energy storage elements. As the illuminance diminishes, so does the harvested electrical energy output. Below a certain threshold, there is simply not enough energy to start up or to run the node with a small solar cell. That threshold depends on the solar cell size and efficiency, and the load it sees during harvesting. There are important considerations to enable energy harvesting and applications to run under low light conditions:

- Use appropriate harvesters. That means solar cells that can harvest sufficient energy at the light levels of the operating environment (compatible with light sources used indoors).
- Ensure low-power cold start. Reduce the amount of energy necessary to start up and keep the harvesting process going. If the energy accumulation process cannot start and be sustained, the system will not cold-start when the stored energy reserves have been used up. Consequently, losses in storage and power management must be kept low.
- Choose low power loads. Reduce the energy consumption of the various loads when the system is active, in order to save energy.

These considerations guided the choice of components to develop or use within the AMANDA project. When meaningful, those components were used for the work presented in this paper. The rest of this document is structured as follows:

- An overview of the state of the art (SoA) related to important components and the SoA of comparable systems is given. The main contributions of this work are listed.
- The system that was designed and tested is described.
- The setup used for the evaluation is described.
- Results of the measurements related to the low-power performance are shown and discussed.
- Future works and a conclusion are given.

For the sake of clarity and focus, Section 2 mostly looks at elements and architectures that could be relevant for case 2 and case 3 mentioned above. That means the possibility to cold-start and run under low light conditions. Measurements are overwhelmingly based on the use of white LEDs as light sources. They are considered a dominant light source indoors. For the sake of completeness, some tests were performed with other light sources, and related measurements are shown at the end of this document. One is dealing here with very low light levels. Thus, results are mostly given with respect to illuminance (lux). Luxmeters are more fitting to measure such levels because they are more sensitive and affordable than pyrometers (irradiance measurement). For solar cells used indoors, manufacturers also often refer to illuminance. The present lack of standards for performance comparison between illuminance and irradiance in indoor settings is known. Suggestions have been made for conversions. However, for meaningful results and comparisons, the spectrum of various elements should properly be taken into account, which adds a serious level of complexity, especially at low light levels [14].

2. State of the Art Review and Main Contributions

For decades, solar-powered pocket calculators have been the flagship examples of indoor solar harvesting. The last few years have seen a trend towards using solar cells for more demanding applications. This is in part related to the availability of better harvesters and electronics that require less energy. For example, Samsung introduced the 2021 Samsung QLED TV remote controls, where solar energy is used as the main power source or to extend the lifetime of a battery [15]. There are now several firms marketing solar cells that can work under low light conditions. Some of the datasheets mention the amount of energy that can be harvested at illuminances as low as 20 lux. This indicates that manufacturers see some potential for energy-autonomous devices that run under poor illumination levels.

2.1. Examples of Some Solar Cells on the Market (the List Is Not Exhaustive)

Several parameters should be considered in the selection of a solar cell for a final product. Some examples are costs, mechanical flexibility, effect of moisture, lifetime, and consequences of the material used on the environment. For the work performed here, only the power output at low light was taken into account. In [16], there is more information pertaining to the advantages and disadvantages of various solar cell technologies.

- Epishine [17] claims $18 \pm 2 \mu\text{W}/\text{cm}^2$ (at 500 lux) in the product brief of their LEH3 devices (warm white LED). For 200 lux, the energy output claim for the technology is $\sim 8 \mu\text{W}/\text{cm}^2$. For 50 lux it is $\sim 2 \mu\text{W}/\text{cm}^2$ [18].
- The BCS4430B6 device from TDK has a surface with dimensions of $44 \text{ mm} \times 30 \text{ mm}$. Its datasheet gives an operating current of $30 \mu\text{A}$ for an operating voltage of 2.6 V at 200 lux [19]. Based on those values, the calculated electrical output per surface unit at 200 lux is $\sim 6 \mu\text{W}/\text{cm}^2$ (illuminated by white fluorescent light).
- Lightricity gives $22.1 \mu\text{W}/\text{cm}^2$ at 200 lux (white LED light) for their EXL1-1V20 solar cell module [20]. The Lightricity solar cell technology is also used for the AMANDA project and for this work.

There are many other manufacturers or start-ups working in that area (PowerFilm, Ambient Photonics, Saule Technologies, etc).

2.2. Solar Cells and Harvesting Architectures

Several efforts have been made to improve the characteristics of various cell technologies that could be used indoors. Juang et al. listed some progress and demonstrated dye-sensitized solar cells (DSSCs) achieving 16.0% efficiency under 200 lux illumination and perovskite solar cells (PSCs) achieving 23.4% efficiency under 200 lux illumination [21]. Biswas and Kim discussed the statuses of different photovoltaic technologies for IoT indoor applications. They listed the characteristics of the different technologies and pointed out the areas where progress is needed [22]. Li et al. gave an overview of the developments of indoor photovoltaic technologies, focusing on organic solar cells, dye-sensitized solar cells, perovskite solar cells, and newly developed colloidal quantum dot indoor solar cells. They also investigated the impact of the characteristics of indoor lighting conditions [23]. Mathews et al. discussed the use of GaAs solar cells indoors and compared them to DSSCs [24].

In addition to solar cells, the power management and the storage element are also very important. Addressing the leakage of storage elements is essential while working at very small illuminances, as it may seriously delay or even prevent cold-starting. Supercapacitors are often used to store energy. One of their advantages is that they allow tens of thousands of charge/discharge cycles, compared to the hundreds of rechargeable batteries. This is crucial if products are to have a long lifetime. However, supercapacitors have relatively high leakage and self-discharge currents. Other storage technologies and power management architectures have been tested [25,26]. Baek et al. use the concept of storage-less and converter-less energy harvesting to power a very small wearable patch designed for monitoring UV exposure outdoors [27]. The system uses a small solar cell. No information is given about the required illuminance. As it is used outdoors, one can assume that the light intensity is not an issue during the day.

2.3. Examples of IoT Systems Powered with Solar Cells (They Mostly Work at 100 Lux or Above)

In 2015, Meli et al., described a BLE-compatible wireless node that is powered using energy harvested using LEDs as harvesters. The accent of that system was on reducing costs by using widely manufactured elements such as LEDs that act as harvesters. The node used a low-power comparator to properly deal with the very small amount of energy coming from LEDs or from photodiodes. In order to further reduce the energy required by the load, a specially engineered (at the integrated circuit level) microcontroller and transceiver were used. Those components are not available on the market. The system required hundreds of lux to work and was meant for outdoors and therefore not suitable for

poorly illuminated places. It also did not include means for synchronous or asynchronous power up [28].

In 2017, Yue et al., developed and tested an indoor photovoltaic energy harvesting module that they used to power a CO₂ sensor. The photovoltaic module had an active surface of 10 cm². The solar cells were connected in such a way that the module delivered the required voltage without the need of a maximum power point tracking (MPPT) device, thus simplifying power management. A supercapacitor was used to buffer the energy, delivering an output voltage of 3.6–4.2 V with a 100 mA pulse current for up to 600 ms. The IoT node was tested at 200 lux, but not at lower illuminance [29].

In 2018, Wu et al. presented a wearable sensor network system for safety applications powered using energy from a round solar panel with a radius of 3 cm (28.27 cm²). The node included several sensors and used LoRa as wireless system. The indoor tests shown were for 600 lux [30].

Also in 2018, a system was presented by Pubill et al. for “Harvesting artificial light indoors to perpetually power a Wireless Sensor Network node,” working down to 500 lux. It used an MP3-25 photovoltaic cell from PowerFilm Solar with a size of 27.36 cm². Energy was buffered using a VL3032 (100 mAh) rechargeable coin battery [31].

In 2020, Kantareddy et al. [32,33] reported a very low-cost node powered using perovskite solar cells. The solar cell had a surface of 1.06 cm². It was used to power an HF RFID tag that communicated with a reader up to 4 m away, using back-scattering communication. The main innovation was in the solar cell, which can allow a variety of applications at low cost. The system should work indoors and outdoors, although there was no mention of the required light levels.

Also in 2020, using a novel co-sensitisation strategy, Michaels et al. tailored DSSCs to power IoT devices capable of artificial intelligence. The reported conversion efficiencies of the cells under ambient light (fluorescent lamp) were: 34%, 103 µW/cm² at 1000 lux; 32.7%, 50 µW/cm² at 500 lux; and 31.4%, 19 µW/cm² at 200 lux. An array with an active area of 16 cm² illuminated with 1000 lux of fluorescent light was used as power source for machine learning on wireless nodes (ATmega328P microcontroller running at 8 MHz, nRF24L01+ transceiver, AVX 6.0 V 0.47 F supercapacitor as energy buffer). The computational needs were met at 1000 lux. However, according to the authors, “the harvested photocurrents follow a linear dependency on the intensity of illumination. As a result, the photovoltaic cells will continue to steadily charge the energy buffer” [34].

In 2021, La Rosa et al. reported an energy-autonomous node powered by an amorphous solar cell (AM-1606C) from Panasonic with a total area of 15 × 15 mm (2.25 cm²). Communication was achieved with a BLE module that transmitted 7-byte ADV frames at +8 dBm on each of the three ADV channels. The 2 ms events required 37 µJ. The solar cell was also used as light sensor. The system was tested down to 200 lux [35].

Also in 2021, Mishu et al. presented a hybrid system where a solar cell and a TEG were used to power a wireless sensor node. The proposed system can run at a minimum of 0.8 V input voltage under indoor light illumination of at least 50 lux and a minimum temperature difference, $\Delta T = 5$ °C [36].

Again in 2021, Elsys advertised a LoRaWAN sensor that is powered with an indoor solar cell and a rechargeable battery. It used an Epishine indoor solar cell [37].

2.4. Systems Working at 30 Lux or Below

The following systems are nearest to the work presented in this paper, in regard to cold-starting and activity at low light and the size of the solar cell.

In 2020, Meli et al., described a LoRaWAN node that could be cold-started at 30 lux. Once started, the node worked down to 20 lux. The node used an 8 cm² solar cell from Lightricity and a power manager from EM Microelectronics (EM8502). Energy was stored in a 10 mF supercapacitor. Measurements of various parameters were transmitted using the LoRaWAN in SF7BW125 mode with +8 dBm RF output power, allowing the coverage of a small building. After a cold start, measurement and communication were possible

every 10 min at low illuminances [38]. The combination of the MCU with serial FRAM (Ferroelectric Random Access Memory) allowed critical LoRaWAN information to be kept even in the absence of power. This enabled the MCU to be switched off in order to optimise harvesting. The critical parameters in the FRAM could be retrieved after powering up in order to allow communication with the LoRaWAN server to proceed with minimal energy. The use of FRAM over FLASH brings significant advantages, as far as energy consumption and lifetime are concerned. Because LoRa requires far more energy than BLE (tens of microjoules against several millijoules, depending on spreading factor and output power), it can reasonably be assumed that the system will also work well with BLE. However, the complex power management and the use of a supercapacitor storage element had a negative influence on the minimal energy level required and thus the size of the solar cell and the lowest illuminance level. The system also required more than 90 min from empty storage until the first frame was sent.

In 2016, Vračar et al. presented a solar power node that could cold-start at 20 lux. The design featured the SLMD600H10 harvester, which is a monocrystalline solar cell with a total area of 35 mm × 22 mm (the active area was about 6 cm²). The node integrated two types of storage elements. The primary storage (a kind of short-term storage) was made up of 2 × 470 µF capacitors. Energy stored there was used for the node or to fill the back-up storage, as long as there was enough energy coming from the solar cell. The back-up storage was a supercapacitor of 1.5 F. It was used when there was not enough energy coming from the harvester (or primary element), providing that enough energy had been saved in it during previous harvesting periods. Comparators were used to determine the levels and to route the path the harvested energy takes. During a cold start condition, harvested energy was used to start an MCU which could subsequently control some of the routing elements. At 3 V, the whole device in sleep mode consumed approximately 6.6 µA (3.7 µA for the harvester, 1.2 µA for the MCU, 1.1 µA for the detector, 0.5 µA for the supercapacitor storage, and 100 nA for the radio). Temperature and humidity data were acquired during the measurements and were transmitted periodically in packets of 12 bytes (1 byte as preamble, 4 bytes as sync word, 1 byte as address, 4 bytes as sensor data, and 2 bytes as CRC) every 5 min [39].

Better performances have been reached on chip level with devices working at very low voltages. In 2020, Lin et al. presented a node capable of operation under moonlight (approximately 1 lux). The special test chip that works around 0.3 V was manufactured using 180 nm technology and was powered by an external 4.1 × 4.1 mm solar cell. It did not require any DC/DC converter and featured an MPPT and a low-power sensor. It dynamically adapted to the harvested power, from nanowatt to milliwatt, with performance proportional to the available power. At 1 lux, the device required 3.1 nW, and the MCU ran computing operations at 7 Hz. At 100 lux, the MCU operated faster, at 18 KHz. At 350 lux, the MCU ran at 75 KHz. The device did not include any transceiver. According to the authors, backscattering is one of the communication methods that could be considered [40].

2.5. Other Components Important in This Work (the List Is Not Exhaustive)

2.5.1. RTC and Low-Power Timers

There are several modules on the market that can be used for timekeeping or for timing. Some combine an RTC integrated circuit and a crystal. This combination helps reduce the size of the module and creates a mechanical unit that adds stability to the device. Several MCUs also integrate RTCs. However, there are important advantages in separating the MCU and RTC [41]. For instance, a stand-alone RTC gives the option of switching off the MCU to further reduce energy requirements, while keeping time in the RTC (a device that usually requires little energy). There are several commercially available examples of low-power RTCs with or without integrated crystals.

- The PCF2131 of NXP is a temperature compensated RTC that can work from 1.2 V to 5.5 V (clock operating voltage) [42]. It typically consumes 64 nA at 3.3 V and can

communicate with a host microcontroller using a serial link. The device does not have any extra memory for user data.

- The RX-8731LC of Epson [43] is a timekeeping module with an RTC and a built-in frequency-adjusted 32.768 kHz crystal. It can work between 1.5 V and 5.5 V and includes 80 bits of EEPROM for user data. The current consumption is typically 350 nA with a maximum of 800 nA at 3 V.
- The devices of the Artasie family of the manufacturer Ambiq (AM0805, AM0815, AM1805, and AM1815) [44] are RTCs that can run using their internal RC oscillator when accuracy constraints are more relaxed. They can also run with an external crystal to provide more accurate timekeeping. They work from 1.5 V to 3.6 V, and their energy requirements depends on the type of oscillator that is used. The lowest current requirement is achieved when the system runs uncalibrated with the RC oscillator (14 nA typical, 220 nA maximum at 3 V). In an intermediary mode, regular autocalibration of the RC oscillator is possible against the crystal oscillator that must therefore be activated. The AM1815 requires 22 nA typically and 235 nA maximum at 3 V. In the most accurate mode, it runs on a crystal. It consumes 55 nA typically, and at the most 330 nA at 3 V. The devices can communicate with a host MCU using a serial link. A 256-byte SRAM memory block is available for user data.
- The TPL5110 of Texas Instruments [45] is a nano timer that consumes 35 nA at 2.5 V (typical) and 50 nA max. It works between 1.8 V and 5.5 V. It can be used to time events. The time interval is set using an external resistance that is read at start-up. The extra energy required at cold start to read the external resistance should be considered, especially when there are frequent cold starts. The manufacturer has other variations of the product, with various features. The TPL5110 is not as accurate as devices that use a crystal.

Most of the devices reviewed above must be initialised by an MCU, which means that the microcontroller must first be powered up to initialise them the first time. In all cases, the current consumption increases if the RTC outputs a signal to drive another device. The current increase depends on the output signal frequency.

2.5.2. Touch Detection

This is a low power method often used to enable user input. Contact with appropriate electrodes generates a signal that can be used to interrupt or wake-up for the MCU. In this way, the MCU can spend much time in the lowest power mode and be activated only when necessary. Capacitive sensing can also be used to measure parameters that are related to capacitance values. The energy consumption of the device monitoring capacitance is important. In many cases, MCU pins are programmed to implement wake-on-touch functionalities. There are also stand-alone devices that implement such functions. The advantage of using MCUs is in the cost and volume savings. However, the CPU must regularly scan the MCU ports, which requires energy and appropriate timing. Most MCU manufacturers have devices or application notes that show how to implement capacitive sensing using their MCUs. Some examples can be found in [46–48].

The energy requirements of the solutions suggested by various manufacturers vary. Hussaini et al., (2017) [49] report values between 3.961 μ W and 0.6910 μ W per button for various MCUs scanning at 8 Hz.

The manufacturer of the EM6420 gives 6 μ W for 16 sensors scanned at 8 Hz [50]. That is 0.375 μ W per button. Generally, full MCU ports are used, meaning that scanning for one button will still require a full port to be programmed. The energy for one button will thus be close to the energy for the port.

Hussaini et al. [49] proposed a very low-power architecture for capacitive sensing that requires only 0.015 μ W per button. Among others, that architecture uses a relaxation oscillator to reduce the requirements of scanning, with the assumption that a very accurate clock is not needed. A commercially available product based on that architecture is not presently known to us.

In applications that require timers or RTCs, further energy reduction is possible by using other types of oscillators. For example, wake-up oscillators requiring only picowatts have been demonstrated [51]. They are less accurate than systems based on crystals but are tolerant of voltage changes and therefore convenient for energy harvesting applications. The final choice depends however, on the use case of the node and sometimes on the availability of the commercial products. Similarly, energy could be saved in the choice of the type of sensors and wake-up techniques needed to trigger the cold start of the node, the use of energy aware techniques [52]. Here also, the requirements the application at hand are important.

2.6. Main Contributions of This Work

To the best of our knowledge, few works related to powering wireless nodes at illuminances below 20 lux have been reported. The main contributions of this work can be summarised as follows:

- An autonomous short-range wireless sensor is designed, capable of cold-starting and working in poorly lit environments, down to 5 lux with a small solar cell module of 4 cm². The node mainly uses commercially available components. This seriously improves on the current state of the art of 20–30 lux using components that can be found on the market.
- Based on the given components, the system is used in a low-power wake-up concept that keeps the high-energy consumers (microcontroller and radio) switched off most of the time. This reduces the load during the harvesting process while allowing sensing and accurate timekeeping to proceed. The MCU can be powered up periodically by an accurate real-time clock (RTC) or asynchronously by a user's touch action. The current consumption of the combined active touch scanner and RTC is below 200 nA at room temperature, allowing them to be powered with very little energy from the harvester.
- The given low-power capacitive sensor can be used for touch detection (detecting the presence of a human body) or to measure parameters that can be related to capacitance values. That device may be configured via an OTP (one-time programmable) to control the energy supply of an embedded system. The sensor can be powered directly with the harvested energy.

The simplicity and small size of the design make it possible to envisage a thin and small node for various applications.

3. Description of the System

Figure 5 shows a block diagram of the hardware. The system consists of four parts:

- (1) The energy harvester module, which in this case is composed of 4 small solar cells.
- (2) The energy store and its monitoring system. The harvested energy is accumulated in a 100 µF capacitor. The amount of energy stored is related to the voltage of the capacitor by $E = 0.5 \times C \times V^2$, where E is the energy, V is the voltage developed across the capacitor, and C is the capacitance. The energy storage is monitored using a low-power comparator. Once the store's voltage reaches a predetermined value, the electronic switch SW1 is activated to allow the stored energy to be used for the wake-up subsystem.
- (3) The RTC and the touch sensor. These are low-power elements used for timing activities (RTC) or as a sensor for applications where capacitive sensing is needed. In this work, they are used to detect a finger touch. The sensors are used to switch on a more demanding load at the convenient time, via switch SW2.
- (4) The MCU and transceiver. The MCU is used to process information and control the application. It is cold-started by a timing pulse from the RTC or by a touch event. The MCU can also communicate wirelessly with other nodes, enabling it to share information. The processing and communication power requirements should be within the available energy budget (that is, the energy delivered by the harvester or stored in the capacitor).

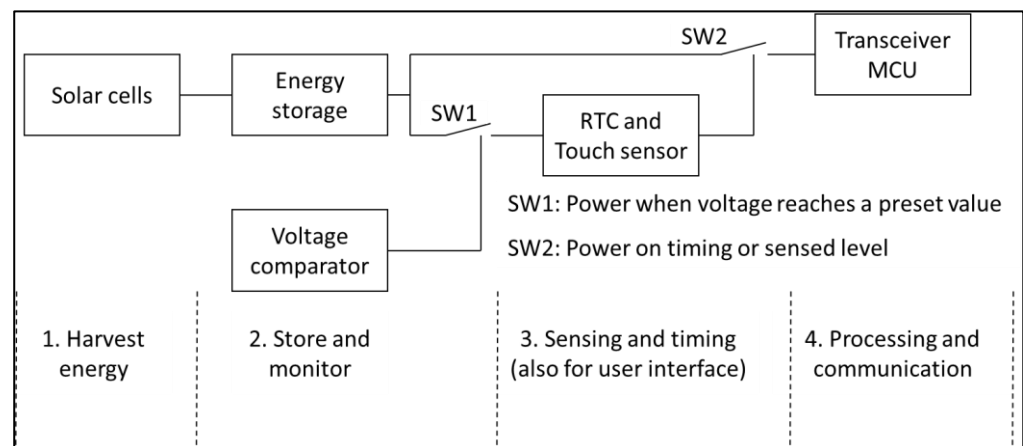


Figure 5. Block diagram of the hardware.

The architecture in Figure 5 shows a generic approach. In order to meet the requirements of a system capable of working at illuminances as low as 5 lux, optimization is required at some key points.

- In general, small solar cells deliver small amounts of energy. This is even more critical at low light intensities. One is here in the realm of hundreds of nanowatts to a few microwatts of input power. As examples:
 - The indoor solar cell manufacturer Epishine report in their datasheet an output of $14 \mu\text{W}$ for a $50 \text{ mm} \times 20 \text{ mm}$ cell, at 50 lux. Assuming a linear relation between illuminance and output power, one reaches $1.4 \mu\text{W}$ @ 5 lux for a 10 cm^2 cell [53]. That is $0.14 \mu\text{W}/\text{cm}^2$ at 5 lux. A 4 cm^2 cell used at 5 lux within a system with 80% energy transfer efficiency will thus deliver 448 nW of power ($0.14 \mu\text{W} \times 4 \times 0.8$).
 - The solar cell manufacturer Lightricity reports $22.1 \mu\text{W}/\text{cm}^2$ at 200 lux for their EXL1 solar cell [19]. Assuming a linear relation between illuminance and power and 80% transfer efficiency, this corresponds to 1768 nW of power for a 4 cm^2 cell at 5 lux ($22.1 \mu\text{W} \times 0.8 \times 4 \times 5/200$).
- The small amount of available energy means that care should be taken to reduce leakages during the harvesting process, to be able to cold-start and reach a voltage level that is necessary for the electronic components to function. To achieve that, the harvesting process is isolated using a switch controlled by the low-power comparator. The current consumption of the comparator and the leakage of the storage have a negative influence on the harvesting process. These elements should therefore be chosen appropriately.
- MPPT is a process that enables the optimal transfer of energy from the solar cell. That process itself requires energy. MPPT is not used here because only a very small amount of energy is expected at low illumination.
- In general, the voltage delivered by the solar cell decreases as the illuminance is reduced. In order to reach the required voltage level, a booster can be used, which often requires additional energy to start up. For example, the EM8500 power management device typically requires $3 \mu\text{W}$ for a cold start and $1 \mu\text{W}$ while running [54]. The AEM10941 power management device requires a minimum of $3 \mu\text{W}$ to cold-start [55]. In this work, the alternative chosen to avoid the relatively high energy requirement of boosters at start-up is to connect several solar cells in series, which leads to additional components.
- The wireless system chosen is BLE. Data can be transmitted in ADV or in connected mode using a certified BLE system-on-chip (SoC). This wireless system requires tens of microjoules per frame while transmitting at 0 dBm [56].

Main Components

Figure 6 shows a schematic of the node.

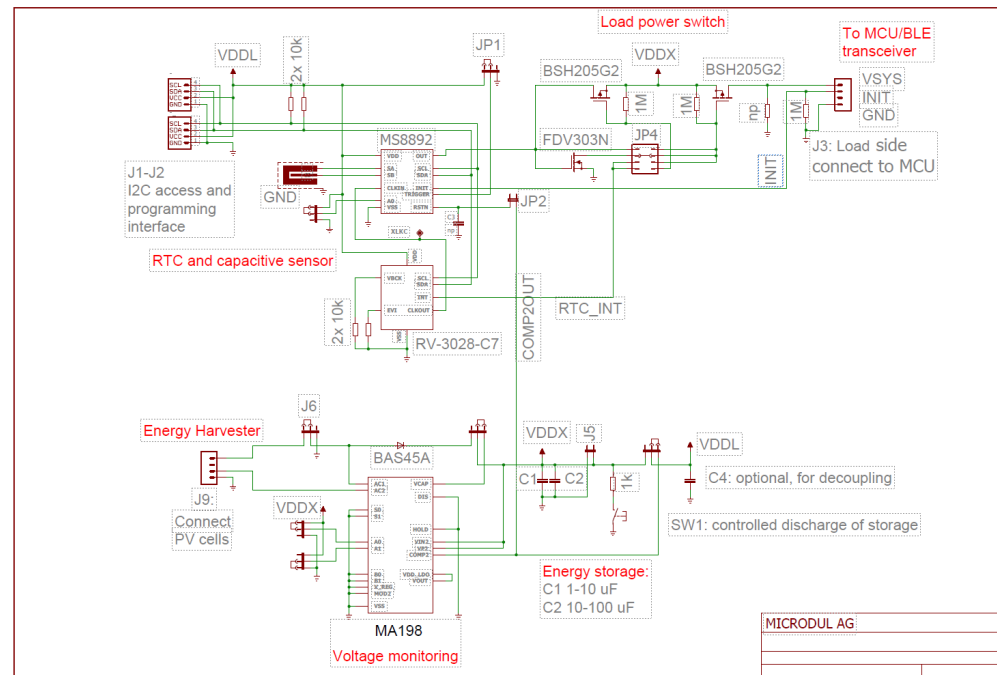


Figure 6. Hardware schematic.

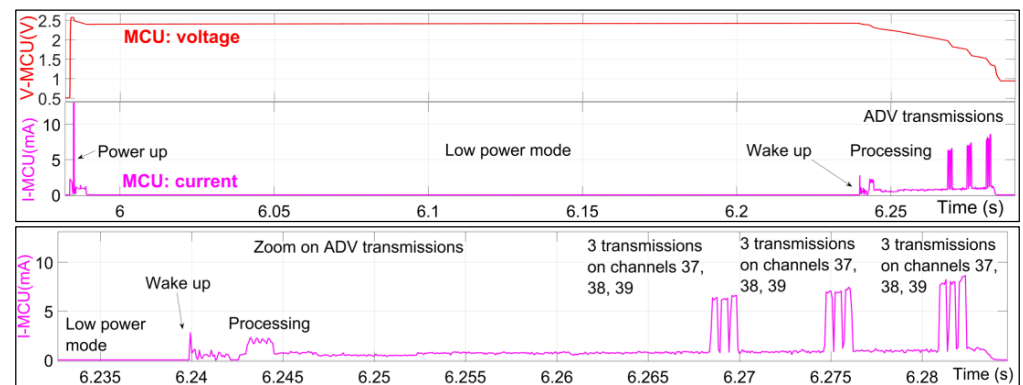


Figure 7. After power up, the MCU advertises several times on all 3 ADV channels. The energy required for the whole sequence is about 135 μ J.

The main components are described below:

- The EXL1-1V20 solar cell [19,57]. The module consists of four EXL1-1V20 cells from Lightricity. Each cell has a surface of 98 mm² (approximated in this work to 1 cm²). The technology enables high indoor and outdoor efficiencies. High-purity III-V material is used for the cells. The lifetime is quoted as above 20 years. According to the manufacturer, no extra diode is needed between the cell and the storage. The energy output at 200 lux is given as 22.1 μ W/cm² (white LED spectrum), for an operating voltage of 1 V and an current of 21.7 μ A. According to the manufacturer, “Lightricity PV technology achieves a conversion efficiency over 35% in the lab, and over 30% in production” [58].
- The MA198 power manager [59]. This is a device from Microdul AG and Algra AG in Switzerland. It was designed for energy harvesting and other low-power applications. It allows a storage element to be charged by an external harvester source, with minimal interference with the final load. In this work, only a single comparator of the MA198 is

used. The comparator monitors the voltage of the storage capacitor and separates the solar cells and storage from the load during the initial energy harvesting process. Once a predefined voltage is reached, energy is allowed to flow into the load. A built-in hysteresis avoids unwanted restart operations. The device typically requires 30 nA at room temperature. In this work, the threshold for detection was set to 2.4 V using external pins (2.25 V measured). The use of the comparator enables the system to harvest and accumulate, even when the power delivered by the solar cell is very small (low light intensities).

- The RV-3028-C7 [60–62]. This low-power RTC module is manufactured by Micro Crystal. It integrates a real-time clock and a 32 kHz crystal quartz, conferring it an accuracy of ± 1 ppm at 25 °C. An integrated EEPROM allows parameters to be configured and re-read, even after a power failure. The device works between 1.2 V and 5.5 V, typically requiring 45 nA at 3 V (60 nA maximum at 3 V). More when driving an external load. The module can work in stand-alone mode, using parameters read from its EEPROM when it powers up. It can also communicate with a host using its I²C bus. It can be programmed to generate interrupts or to control other circuits. In this work, the RV-3028-C7 is foreseen as a low-power accurate timer, capable of starting the embedded system at defined time intervals. It also generates a synchronous signal that pilots the capacitive touch sensor. That leads to a lower current consumption than if the touch sensor is clocked internally. Low power consumption in active mode is important. The energy requirements at cold start are also fundamental, as they affect the amount of energy that should be accumulated before a cold start is possible.
- The MS8892 capacitive touch sensor [63]. This device is an ultra-low-power capacitive sensor and touch switch for human body detection and system wake-up. The device incorporates a memory latch to keep the power state active until the system controller decides to shut down the active power once the processing and communication tasks are completed. The flexible and fully configurable output logic of the MS8892 also allows setting the power-state latch by external wake-up sources (like the RTC in the present architecture, or other wake-up sources). A selectable absolute or relative capacitive switching threshold allows for compensation for material and fabrication variations of the sensor electrodes. With an active power consumption of 720 nA in stand-alone operation and 65 nA when clocked externally, the MS8892 is optimally suited as an ultra-low-power system power controller and many other applications where energy is a limited resource. At 3 V, that is 195 nW (external clock energy not counted). In the AMANDA project, the MS8892 is used to enable asynchronous user interaction. By touching the sensor electrodes, the user can trigger a wake-up from the lowest-power mode. The device then routes power to the MCU system, allowing it to cold-start. After powering up, the capacitive touch sensor remains active and is used for user interaction with the system. The ability to configure many parameters of the RTC and the capacitive sensor in non-volatile memories (respectively EEPROM and OTP) enables the selection at cold start of certain system functions, without the need to first start and use the microcontroller. This in turn adds an important flexibility and low-power dimension at start up.
- The RSL10 microcontroller with BLE transceiver [64–66]. The RSL10 is an SoC that integrates a Cortex-M3 microcontroller and a BLE transceiver. The device is Bluetooth® 5.2-certified and supports various proprietary transceiver modes. It also has DSP functionality and support for 802.15.4 wireless protocols. It is used as a BLE controller in the AMANDA project. Bruetsch et al., measured the energy performance of several BLE transceivers in different communication modes [56]. Their work details the energy requirements in different communication modes. The paper demonstrated that the RSL10 has a good energy performance, requiring just tens of microwatts to transmit full ADV frames (advertisement mode). According to the authors, it is possible after optimisation to cold-start the RSL10 and transmit one ADV packet of 47 bytes per frame with less than 30 μ J. The device is also sold in a system-in-package (SiP) fashion, where

the SoC and some of the required components, such as crystals, antenna, capacitors, and others are in a single space-saving package. This work uses the RSL10-SIP-001GEVB development board integrating the RSL10 SIP. The load is powered using the harvested energy. The MCU is programmed to behave as described below:

- Upon power-up, a minimal check is made, and some registers are initialised.
- The MCU then goes into deep sleep mode for about 250 ms, where its current consumption is reduced.
- After the deep sleep, the device initialises its BLE radio and starts ADV_NONCONN_IND advertising events.
- Packets are advertised on channels 38, 39, and 40, with the RF output power programmed for 0 dBm. The transmitted frames have a length of 39 bytes, or 47 bytes in total when the overhead and preamble are counted. Figure 7 shows the corresponding energy trace, captured while powering the programmed RSL10 with the measurement tool.

The RTC was programmed by writing the appropriate values in its EEPROM to enable the 1024 Hz clock output function. The touch sensor was programmed by writing the appropriate values in its OTP to enable the following functions:

- External clock source, 1024 Hz.
- Periodic sensing, $8 \times /s$. Output polarity setting.
- Relative threshold mode with the threshold set to 0×0 A.

Several parameters of the RTC and the touch sensor can be changed under the control of the MCU. In this evaluation, the initial values programmed in the EEPROM (RTC) and the OTP (touch sensor) are good enough for the basic tests. Figure 8 shows a picture of the assembled system with all its components.

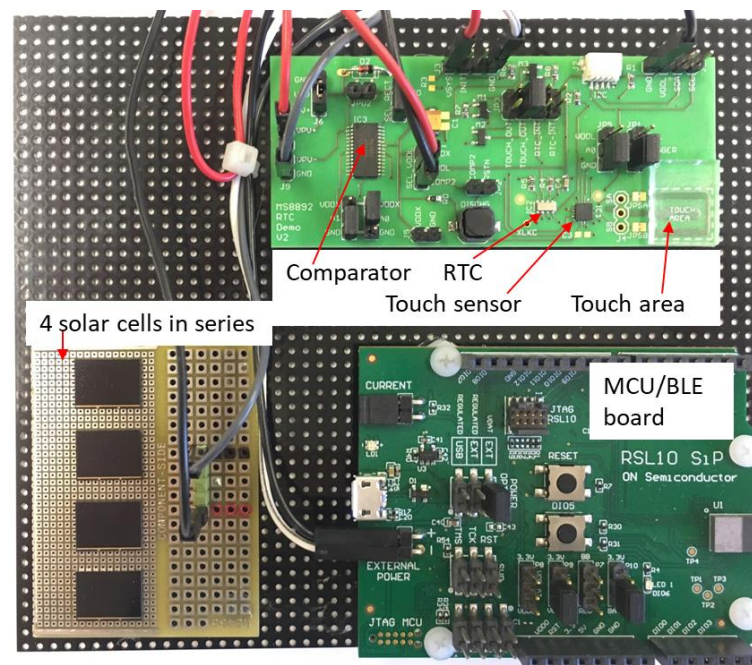


Figure 8. View of the system with different boards connected.

4. Setup

Figure 9 shows the measurement setup used in most cases.

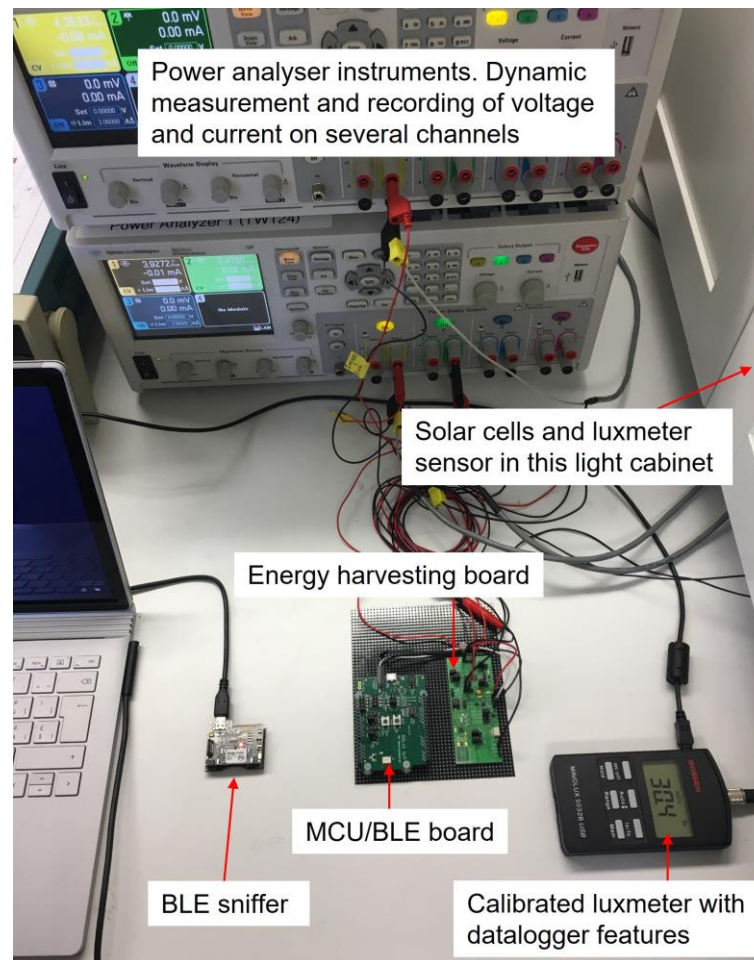


Figure 9. Elements used for the tests.

The main elements of that setup are listed below:

- The power analyser: N678xA from Keysight [67]. Up to two instruments were used in order to have enough channels to measure and log various parameters simultaneously. Voltages and currents at different stages of the architecture were measured, and the power and energy were calculated directly by the instrument. Most measurements reported here were made with the power analyser.
- The luxmeter: a calibrated Mavolux 5032B USB [68]. This instrument was used to monitor and to log the illuminance.
- The BLE sniffer from Texas Instruments [69]. It was used to capture BLE frames (ADV frames for this work). Only one channel was sniffed at the time. The results shown in this paper for ADV channels therefore only relate to one ADV channel, although frames were sequentially transmitted on all three channels.
- The connected boards with the following elements:
 - The solar cell module.
 - The energy harvesting board with the comparator, RTC, and touch sensor.
 - The MCU development board with the RSL10 SiP device.
- The light cabinet. For the tests, the solar cells and the luxmeter's sensor were kept in a chamber illuminated using white LEDs, as shown in Figure 10. The intensity of the LEDs was controlled using an appropriate external power supply. A luxmeter was used to set the desired light intensity and to log its value during the tests. There is a glass between the LEDs and the device under testing and luxmeters, which helps in setting small intensities but also has an impact on the light characteristics. The walls are reflective, which is fitting for many indoor operating environments.

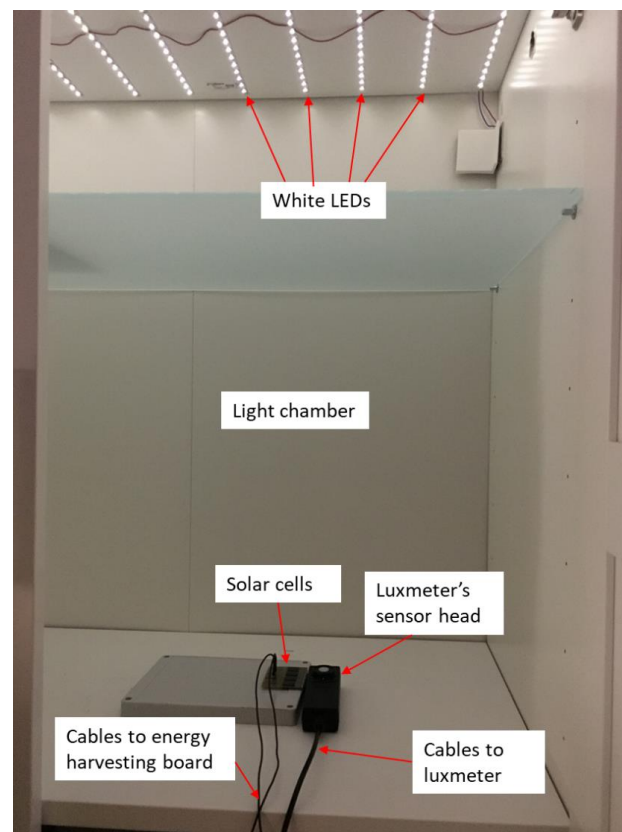


Figure 10. Chamber used to illuminate the solar cells.

5. Results

This section presents results from measurements and tests.

5.1. Measurements on the Solar Cell Module

The characteristics of solar cells at very small illuminances are not always documented. For that reason, the cells used in this work were evaluated to determine their behaviour. The four EXL1-1V20 small solar cells were connected in series, with a variable resistance as load. They were illuminated in the light chamber, and their current was measured. Variable resistance was used to determine the maximum power point (MPP) at various light intensities. The measured and calculated values are reported in Table 1.

Table 1. Measured and calculated parameters of solar cell module at MPP in function of illuminance.

Illuminance (Lux)	2	4	10	19	50	100	200	500
Power (μ W)	0.52	1.05	2.62	5.15	14.92	29.73	63.13	162.2
Load (kOhm)	17,000	9500	4100	2200	850	440	230	95
Voltage at MPP (V)	2.96	3.15	3.28	3.37	3.56	3.62	3.81	3.93

The relation between the matching resistance and the illuminance at low light levels is non-linear. The maximum voltage delivered by the cell decreases with the illuminance and is non-linear at small light intensities. These are the characteristics when the solar cells are optimally loaded. These are different without MPPT.

5.2. Results at 5 Lux

To evaluate its performance, the system was illuminated with the appropriate light intensity, and different parameters were measured and logged for further analysis. The

harvesting board was connected to solar cells and to the RSL10 embedded system. The solar cell module was placed in the light cabinet and the illuminance adjusted to the needed value. The power analyser was set as follows:

- Measure the current from the solar cell (I-SC) and its voltage (V-SC or VDDX).
- Measure the voltage of the sensor and RTC (V-SENS or VDDL).
- Measure the load current (I-MCU) and the voltage of the MCU (V-MCU or VSYS).

The storage capacitor was first discharged. From that time, the system started a harvesting cycle. Shortly after the sensor and RTC were switched on by the comparator (observed on the V-SENS), the sensor area was touched with a finger to start the MCU. The electrical elements of the basic measurement circuit are shown on Figure 11.

- I-SC and V-SC are the current from the solar cell and the voltage of the same, respectively.
- The storage capacitor has a self-discharge represented here by I-SDIS. It is charged with the current I-STOR. Its leakage is represented by I-SLEAK.
- The comparator needs power to monitor the storage capacitor. This is represented by I-CMP. When the comparator threshold voltage is reached, it enables the supply of voltage to the touch sensor and the RTC V-SENS. The devices consume a current I-SENS.
- The touch sensor and the RTC are used to control the power supply of the MCU load. The control elements are biased with I-CTR.
- The current in the MCU load is represented by I-MCU.
- At 2 V, the comparator typically requires $I\text{-CMP} = 30\text{ nA}$.
- The self-discharge of the storage capacitor measured at 2 V is approximately 15 nA.

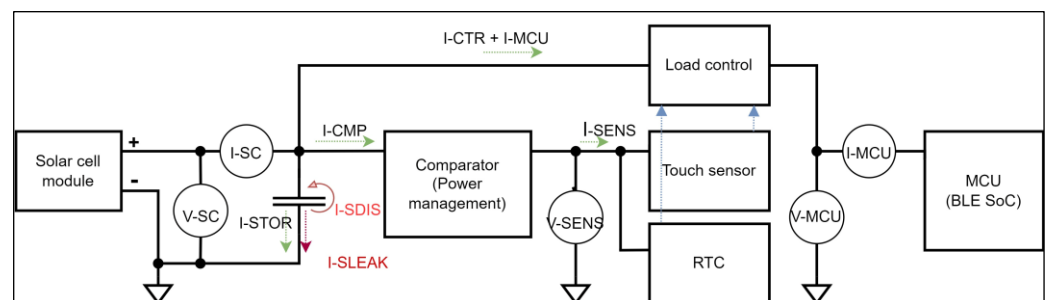


Figure 11. Measurement circuit.

Figure 12 shows a run where the power analyser records the solar cell module's voltage and current, the sensor voltage, and the MCU voltage and current. For the sake of explanation, the main events are marked by letters A to E. The important information for this part is shown by the voltage traces. The electrical current information mostly helps reference peak activities and does not show any detail in this figure. More information about the events is given later, including energy information.

In what follows, the different events are first described. Measurement tables and graphs related to the different phases are then shown and explained. The comparator threshold set to 2.4 V (datasheet value) is measured as 2.25 V.

- Event A: The energy storage is discharged. The storage is manually emptied before the evaluation of the harvesting process begins. As the solar cell delivers energy, the storage voltage goes up. The comparator powers up with it and starts monitoring the storage's voltage. As long as the voltage is below 2.25 V, the load on the solar cell only consists of the storage capacitor, the monitoring comparator, and small leakages. The RTC, sensor, and MCU are all switched off. The voltage of the storage element continues to climb.
- Event B: The touch sensor and RTC are powered on. The threshold of the comparator is reached. The RTC and touch sensor are powered on, leading to a small voltage drop at B. After initialising, they are ready and active. The RTC generates the required clock signal for the touch sensor so that it can regularly compare the capacitance on its

electrode inputs to the threshold and detect whether a touch action has occurred. The harvesting process continues, with the RTC and the touch sensor active. The voltage of the storage increases further.

- Event C: Touch detection and activation of the wireless MCU. System switches off. The touch activity is detected when a finger is placed on the electrodes. The sensor node routes power to the RSL10. The MCU starts up and transmits several frames. That process requires significant amounts of energy. The storage delivers that energy in a short time, and its voltage drops. The MCU activity continues until the storage voltage drops below the comparator threshold. The comparator cuts off the supply of both the timer and the touch sensor and thus of the MCU. The harvesting process continues from point C, and the voltage at the storage goes up again.
- Event D: The touch sensor and RTC are powered on. The voltage of the energy storage element has now reached the threshold set in the comparator, as in situation B. The sensor and the RTC are powered up and restart. The sensor is active and monitors the capacitance at its input pins. Harvesting continues, and the voltage of the storage goes up.
- Event E: End of sequence. As long as there is enough energy from the solar cell, the voltage goes up until it settles, and the capacitive sensor continues measuring the capacitance at the electrodes.

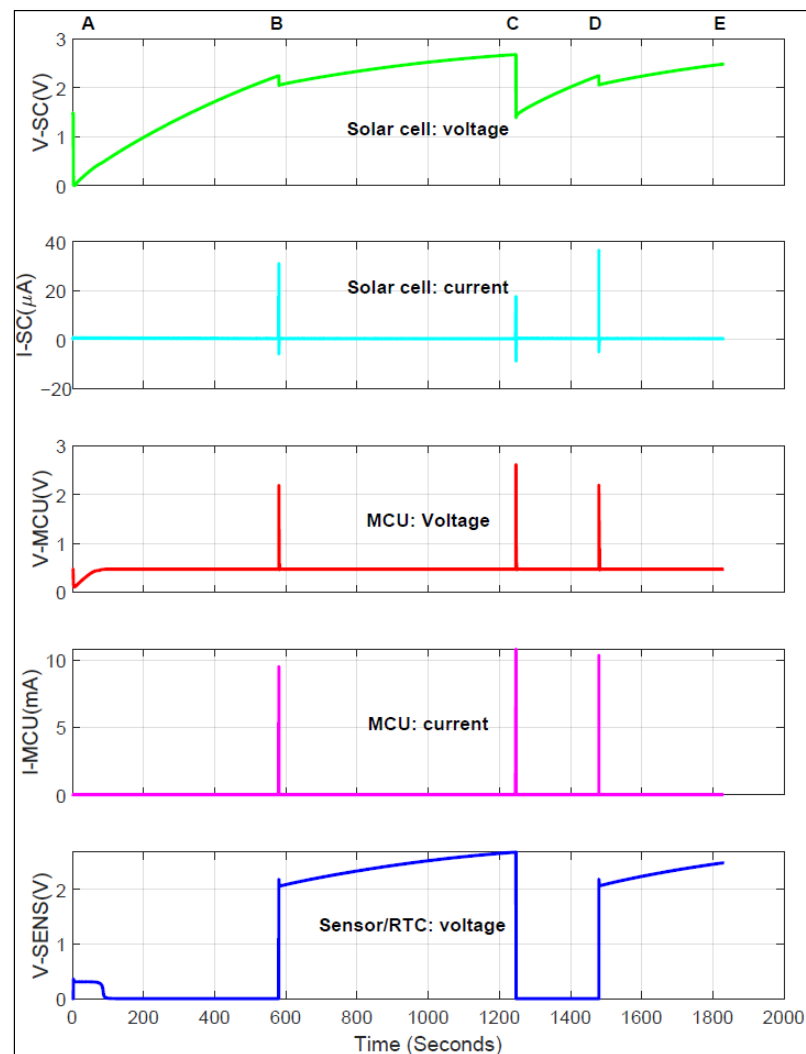


Figure 12. Behaviour at 5 lux (A, B, C, D, E represent times when special events occur).

The tables below show measurements of some of the electrical parameters. The values have been rounded with respect to the numbers delivered by the tool to make the tables easier to read.

- A > to < B: Measurements shortly after A (M1) and shortly before B (M2) (Table 2). The average power delivered by the solar cell in this time slot is $P_{SC} = 566 \text{ nW}$, with peaks of $1.14 \text{ }\mu\text{W}$. The total energy added during this time ($T = 577.688 \text{ s}$) to the storage can be calculated as: $0.5 \times 100 \text{ }\mu\text{F} \times ((2.25 \text{ V})^2 - (1.03 \text{ mV})^2) = 253 \text{ }\mu\text{J}$. In the same time slot, $326.33 \text{ }\mu\text{J}$ is harvested. It means that an amount of $73.33 \text{ }\mu\text{J}$ is harvested but not added to the storage. It is lost in various leakages (the energy capacitor, the comparator, and the transistors in the control stage that deliver power to the MCU). The system requires less than 10 min at 5 lux to cold-start and be ready for operation.
- Signals at event B: Figure 13 shows a magnification of the signals around the position of event B. During its start-up phase, the touch sensor shortly powers the MCU, which starts up and consumes some energy ($30 \text{ }\mu\text{J}$ in 280 ms). This is seen on the signals V-MCU and I-MCU. Thanks to the programmed firmware delay, the MCU goes into a power-saving mode and does not process or transmit any frame. After booting, the MCU power is removed, and the sensor and RTC are active. The touch sensor then regularly measures the capacitance at the electrodes to check for a finger presence.
- B > to < C: Measurements shortly after B (M1) and shortly before C (M2) (Table 3). The average power delivered by the solar cell in this time slot is 856 nW , with peaks of $1.26 \text{ }\mu\text{W}$. In this phase, the energy is consumed by leakage in the storage, leakage in the power stage, the comparator, the RTC, and touch, as the RTC and touch are also active in this time window.
- Signals at event C: Figure 14 shows a magnification of the signals at position C. The MCU is powered on (time 1246.65 s). Initially, much current is drawn, which corresponds to the cold start of the MCU. After the sleep delay implemented in the firmware, the MCU wakes up (time 1246.9 s), goes into processing mode, and transmits ADV frames. Frames are sent until the MCU is turned off. The activities of the MCU last 335 ms and require a total of $262 \text{ }\mu\text{J}$. They are divided into $34 \text{ }\mu\text{J}$ from power on until wake up from sleep, $48 \text{ }\mu\text{J}$ until the start of first frame, and $180 \text{ }\mu\text{J}$ for transmitting all the ADV events. Data transmitted during the ADV events are received by the sniffer (Figure 15). The same information is sent on the three ADV channels for each event. Because the sniffer only scans one ADV channel, 8 frames in total are received. The events correspond to the current peaks seen on the I-MCU current trace (Figure 14). The RSSI (received signal strength indicator) calculated by the sniffer has a value of -37 dBm for all frames (the sniffer acting as receiver is not far away from the transmitting device, as can be seen on the setup (Figure 9)). Figure 16 shows the structure of an ADV frame that is sent. The PDU (protocol data unit) has 39 bytes, corresponding to an on-air frame size of 47 bytes at 1 Mbps . In the best case, all 3 ADV frames of each event are transmitted, which means $8 \times 3 = 24$ frames. In the worst case, the last 2 frames of the last event (channel 38 and channel 39) are not transmitted. That means 22 frames are transmitted. Therefore, the energy harvested is enough to transmit at least 22 frames with a total of 47 bytes each.
- C > to < D: Measurements shortly after C (M1) and shortly before D (M2) (Table 4). The average power delivered by the solar cell is 765 nW in this time slot, with a peak of $1.13 \text{ }\mu\text{W}$. Here, the voltage has gone below the comparator's threshold, meaning that the RTC and the touch sensor are no longer powered. However, the storage capacitor is already at 1.44 V . Current consumption is due to leakage in the storage, power stage, and supply current of the comparator. The RTC and the touch sensor are not active. The storage is being charged.
- Signals at event D: At event D, the comparator threshold is reached, and the touch sensor and RTC are powered. The system behaves as in case of event B. The energy storage was not fully discharged at event C. Therefore, event D is reached faster (here, 231 s). It means that the system reacts faster once it has been started. The application

firmware can be written so as to switch off the MCU earlier and avoid that the RTC and touch sensor be switched off. That would allow the system to react even faster. In the case that the RTC is used for timekeeping, time information would not be lost. The RTC itself can accept a backup storage element that allows it to keep information for a certain time, even when power is not available. That feature was not used in this work.

- D> to <E: Measurements shortly after D (M1) and shortly before E (M2) (Table 5). The average power delivered by the solar cell is 841 nW in this time slot, with a peak of 1.21 μ W. The power consumption is due to leakages and supply currents of the comparator, RTC, and touch sensor because those elements are active. The voltage of the storage capacitor goes up.

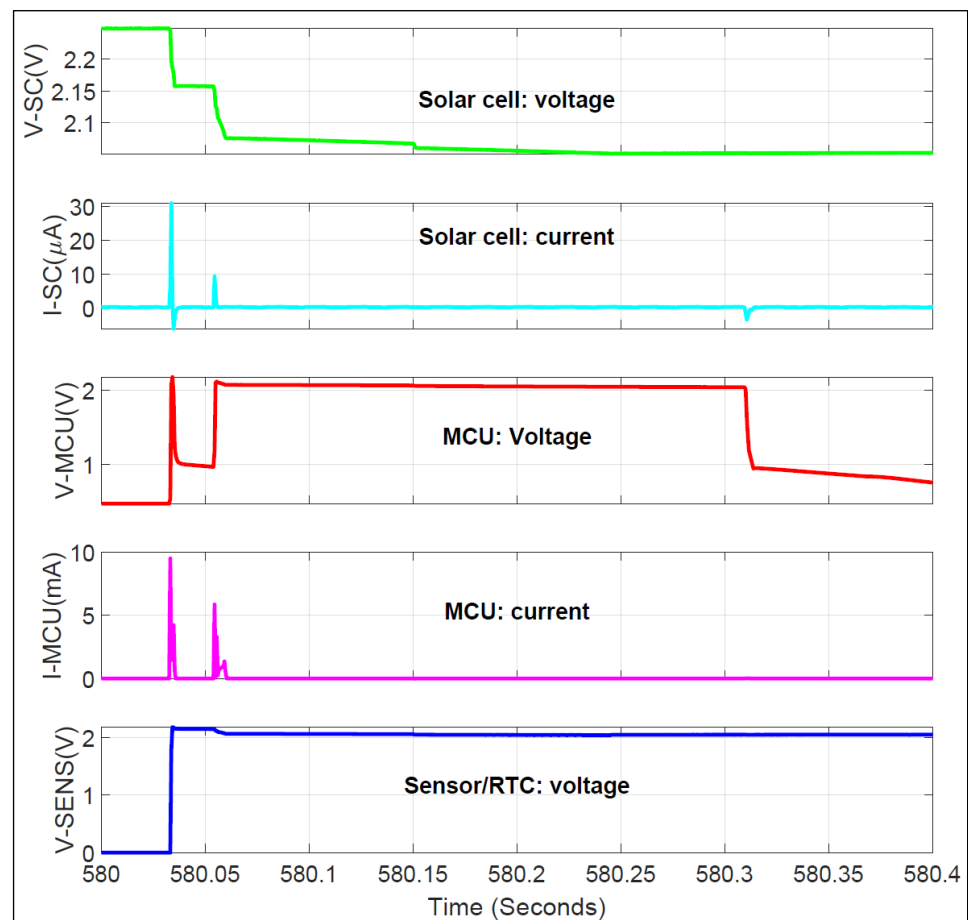


Figure 13. Magnification at event B.

Table 2. Parameters between A and B at 5 lux.

	M1		Measurements between Markers			M2
Time	3.339715 s		$\Delta = 09:36.688620$ (576.688 s)			09:40.028334
	Avg	Min	Avg	Max	Energy	Avg
V-SC	2.54 mV	1.03 mV	1.28 V	2.25 V	-	2.25 V
I-SC	652 nA	246 nA	475 nA	754 nA	-	345 nA
P-SC	2 nW	558 pW	566 nW	1.14 μ W	326.33 μ J	776 nW

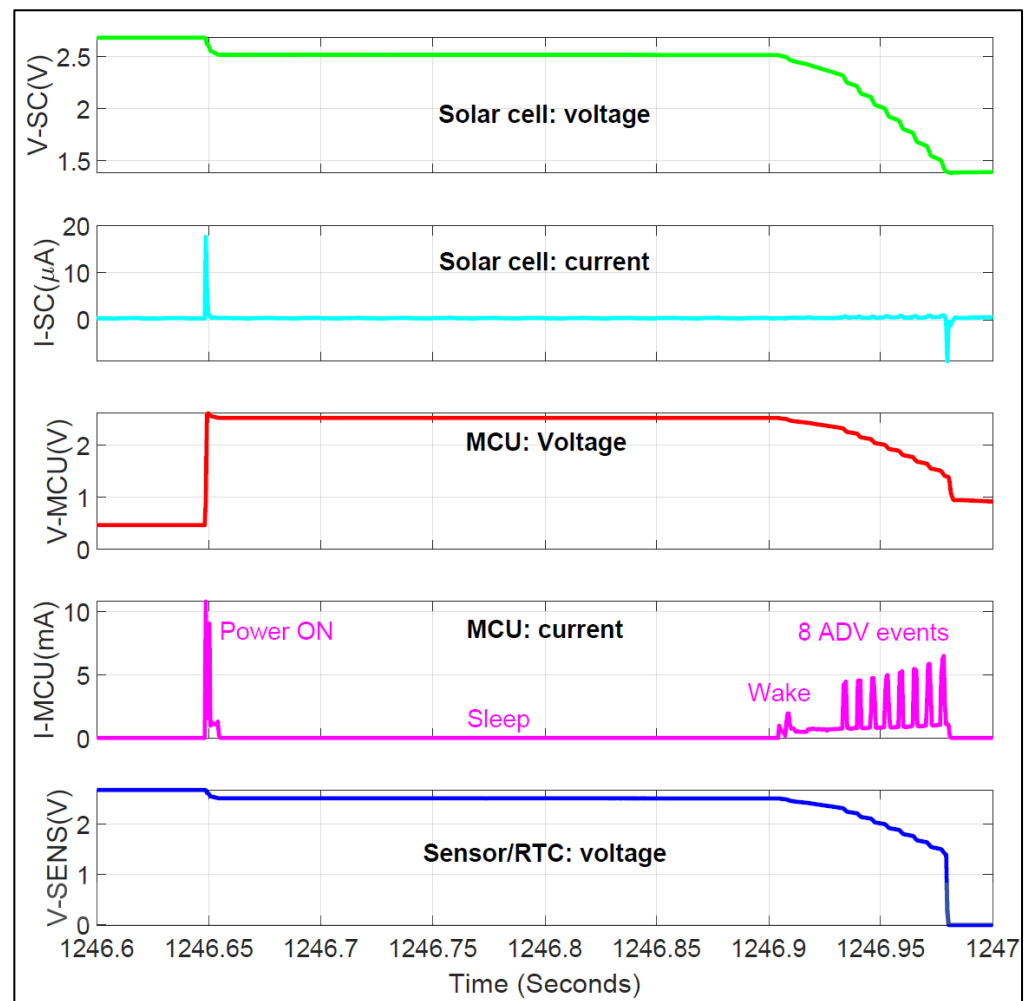


Figure 14. Magnification of event C.

```

42 25 94 11 22 ff ff f5 02 01 04 1b 09 41 4d 41 4e 44 41 5f 31 32 33 34 35 36 37 38 39 41 42 43 44 45 46 47 48 49 4a | -37
42 25 94 11 22 ff ff f5 02 01 04 1b 09 41 4d 41 4e 44 41 5f 31 32 33 34 35 36 37 38 39 41 42 43 44 45 46 47 48 49 4a | -37
42 25 94 11 22 ff ff f5 02 01 04 1b 09 41 4d 41 4e 44 41 5f 31 32 33 34 35 36 37 38 39 41 42 43 44 45 46 47 48 49 4a | -37
42 25 94 11 22 ff ff f5 02 01 04 1b 09 41 4d 41 4e 44 41 5f 31 32 33 34 35 36 37 38 39 41 42 43 44 45 46 47 48 49 4a | -37
42 25 94 11 22 ff ff f5 02 01 04 1b 09 41 4d 41 4e 44 41 5f 31 32 33 34 35 36 37 38 39 41 42 43 44 45 46 47 48 49 4a | -37
42 25 94 11 22 ff ff f5 02 01 04 1b 09 41 4d 41 4e 44 41 5f 31 32 33 34 35 36 37 38 39 41 42 43 44 45 46 47 48 49 4a | -37
42 25 94 11 22 ff ff f5 02 01 04 1b 09 41 4d 41 4e 44 41 5f 31 32 33 34 35 36 37 38 39 41 42 43 44 45 46 47 48 49 4a | -37

```

Figure 15. Structure and contents of the transmitted frame.

Table 3. Parameters between B and C at 5 lux.

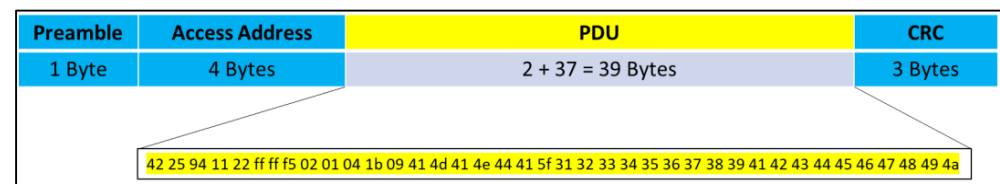
	M1		Measurements between Markers			M2
Time	09:40.398940		$\Delta = 11:06.243236$ (666.243 s)			20:46.642176
	Avg	Min	Avg	Max	Energy	Avg
V-SC	2.05 V	2.05 V	2.42 V	2.68 V	-	2.68 V
I-SC	406 nA	177 nA	354 nA	535 nA	-	288 nA
P-SC	834 nW	468 nW	856 nW	1.26 μ W	570.04 μ J	771 nW

Table 4. Parameters between C and D at 5 lux.

	M1	Measurements between Markers				M2
Time	20:48.623002	$\Delta = 03:50.908887$ (230.908 s)				24:39.531889
	Avg	Min	Avg	Max	Energy	Avg
V-SC	1.44 V	1.44 V	1.89 V	2.25 V	-	2.25 V
I-SC	430 nA	249 nA	408 nA	583 nA	-	344 nA
P-SC	618 nW	462 nW	765 nW	1.13 μ W	176.65 μ J	774 nW

Table 5. Parameters between D and E at 5 lux.

	M1	Measurements between Markers				M2
Time	09:40.398940	$\Delta = 11:06.243236$ (666.243 s)				20:46.642176
	Avg	Min	Avg	Max	Energy	Avg
V-SC	2.06 V	2.06 V	2.30 V	2.49 V	-	2.49 V
I-SC	345 nA	205 nA	367 nA	547 nA	-	319 nA
P-SC	710 nW	460 nW	841 nW	1.21 μ W	293.89 μ J	794 nW

**Figure 16.** Frames captured by the sniffer on one ADV channel.

5.3. Results at 20 Lux

Figure 17 shows a recording at 20 lux. The values delivered by the measurement tool are shown in the Appendix A. There are several harvesting, detection, processing, and communication cycles. At this illuminance, the storage capacitor is charged at up to 3.7 V (Marker 2). The RTC and touch sensor have already been switched on just before the position of Marker 1. The flattening of the voltage curve shows that the maximum voltage is being reached for that illuminance.

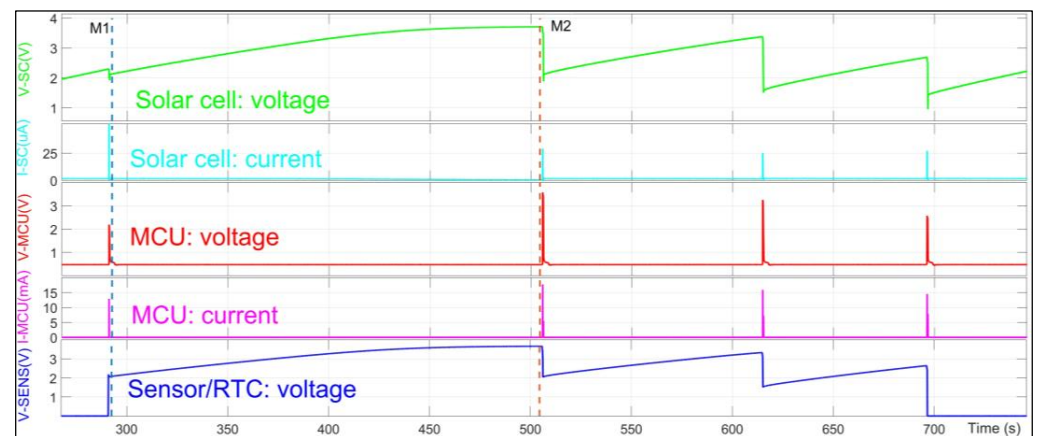
**Figure 17.** Several harvesting, detection, processing, and communication phases at 20 lux.

Figure 18 is a magnification showing the RSL10 current. After the MCU is powered on, 15 ADV events are transmitted, and then the RSL10 goes into low-power mode. The

voltage is still high enough to maintain the RTC and the touch sensor as active and measuring, waiting for the next touch activity. The storage voltage is high enough to allow all programmed 15 ADV events (45 frames) to be sent without completely emptying the storage (Marker M2 at about 2 V). The MCU is switched off by the touch sensor when the finger is no longer detected. The regular current peaks on I-SENS have a frequency of 8 Hz, which is the scanning frequency of the touch sensor. I-SENS is about 170 nA between the peaks, indicating the current consumption of the combined RTC and touch sensor elements.

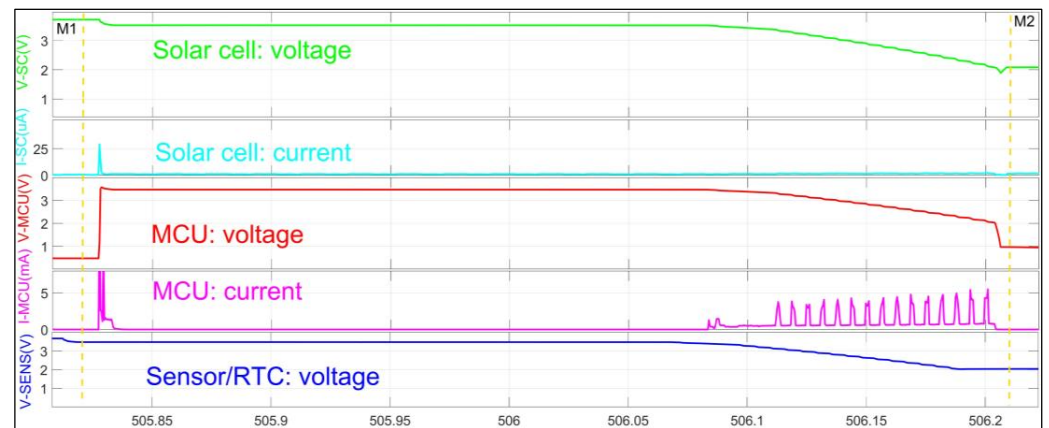


Figure 18. Magnification of a region where the MCU is active at 20 lux.

5.4. Energy Requirements of Touch and RTC

The energy requirements of the combined RTC and touch sensor were measured in another setup. One channel of the power analyser was configured to monitor the voltage applied to the RTC and touch sensor and the resulting current, as shown by Figure 19. The values delivered by the measurement tool are shown in the Appendix A.

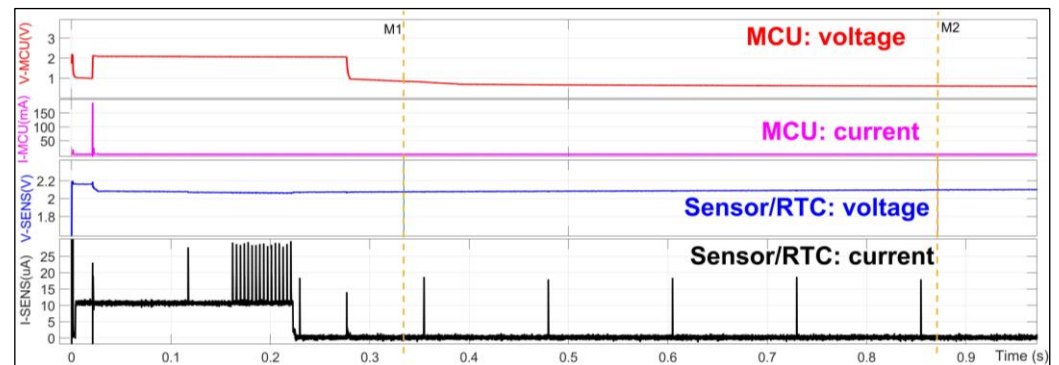


Figure 19. RTC and touch sensor cold start behaviour.

The 8 Hz current peaks between the markers come from the touch sensor, which scans every 125 ms for a finger presence. An average of 164 nA of current is drawn by the RTC and the touch sensor (between markers) at 2 V. That current is 135 nA without pulses, meaning that the measurement pulses contribute to about 20–30 nA more current. This corresponds to an average power of 342 nW. The current increases as the voltage goes up.

Figure 20 shows a magnification of what happens just after power is applied to the touch sensor and the RTC in the first 230 ms (between the markers); 5 μ J is the energy consumed in that phase. The average current is 10.4 μ A. The RTC reads the contents of its EEPROM and initialises accordingly. That results in a high current peak. The touch sensor also initialises using the values it reads from its internal OTP. Because the RTC is not yet delivering pulses, the touch sensor uses its internal clock. The RTC then starts generating clock pulses at a higher frequency before switching to the programmed frequency. When

the touch sensor detects the RTC pulses, it stops using its internal timer and switches to the external clock from the RTC.

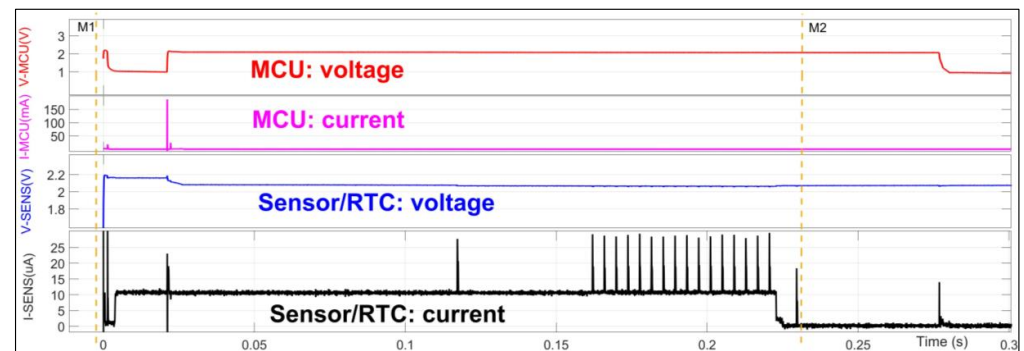


Figure 20. RTC and touch sensor cold start behaviour (magnification).

5.5. Harvested Energy at Different Illuminances

In order to compare the harvesting performance at different low light illuminances, measurements were taken for those light levels. The harvested energy needed to load the storage capacitor from 1 V to 2.2 V was extracted. Table 6 shows the important values as extracted from the measurements—current (I-SC) and power (P-SC). Because the storage capacitor is 100 μ F, the energy change in the storage between 1 V and 2.2 V can be calculated as: $0.5 \times 100 \times ((2.2)^2 - (1)^2) = 192 \mu$ J. The amount of extra energy that is harvested but not stored can be calculated by subtracting 192 μ J from the total energy harvested in the measurement period.

Table 6. Measured parameters as functions of illuminance.

	2 Lux	5 Lux	10 Lux	20 Lux
Start time ¹	04:24.488141	03:20.915354	01:49.326336	01:07.183411
Duration ²	10:14.418022	05:55.556065	02:50.100326	01:20.592077
P-SC Min	212 nW	382 nW	749 nW	1.567 μ W
P-SC Avg	436 nW	702 nW	1.374 μ W	2.758 μ W
P-SC Max	731 nW	1.145 μ W	2.113 μ W	4.13 μ W
I-SC Min	98 nA	236 nA	589 nA	1.422 μ A
I-SC Avg	268 nA	435 nA	855 nA	1.719 μ A
I-SC Max	451 nA	651 nA	1.107 μ A	2.029 μ A
SC energy ³	267.68 μ J	249.578 μ J	233.778 μ J	222.256 μ J
Extra energy ⁴	75.68 μ J	57.578 μ J	41.778 μ J	30.256 μ J
Cold start time ⁵	878 s	556 s	279 s	147 s

¹ This is the time when the energy storage voltage reaches 1 V; ² Duration taken for the energy storage voltage to reach 2.2 V, measured from start time; ³ Energy from the solar cell module in the measurement period (duration);

⁴ Difference between the energy from the solar cell and that in the storage; ⁵ Approximate time from storage capacitor empty (0 V) until sensor ready (about 2.2 V). Min values or Max values do not necessarily occur at the same time. They represent the minimum or maximum in the measurement period.

The harvested energy is similar in each measurement, which is to be expected, as the same storage is charged up to the same voltage (same energy). At lower illuminance values, the harvested energy increases slightly due to the losses over the longer harvesting times. Thus, the duration of harvesting required to fill the storage is also of interest. The values can be read from the table as the time between the markers.

Figure 21 shows the values above, compared to the maximum achievable power output, based on the measurements we made at the MPP. As can be expected, the power is

not optimally harvested. The lack of MPPT allows the system to cold-start and for energy to be harvested at such low illuminance values. This comes at the cost of efficiency. The storage capacitor, that is, the main load seen by the solar cells, has a complex impedance, which means that the current of the solar cell varies as the device is charged.

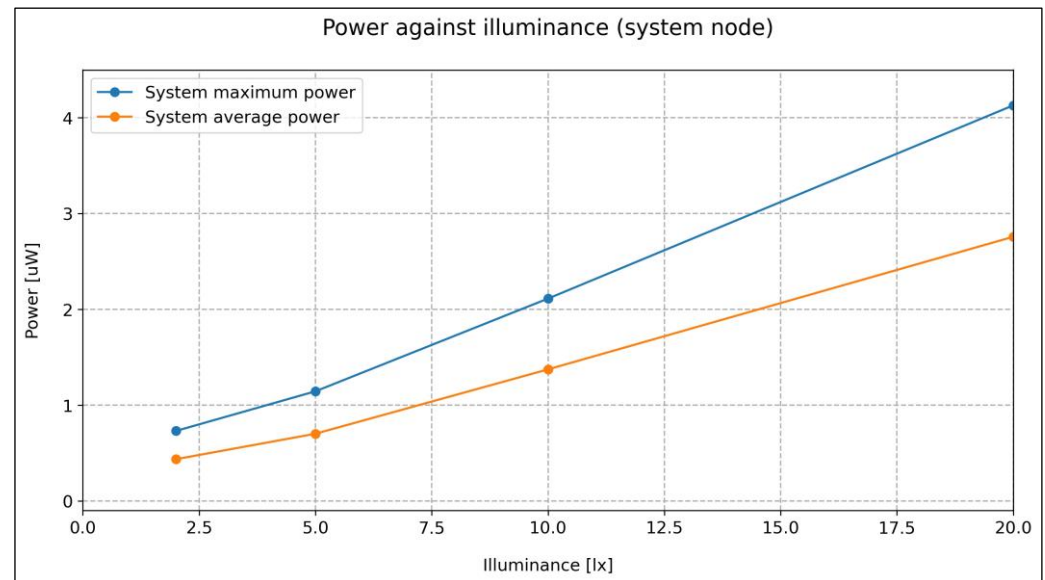


Figure 21. Maximum power and achieved harvested power (LED as light source).

The blue curve (system maximum power) represents the energy that was measured with an optimal load (resistive). The manufacturer's data of $22.1 \mu\text{W}/\text{cm}^2$ is given at 200 lux. No datasheet information for lower illuminances is available. The differences in the spectra of the light sources will also make comparison difficult.

Considering the energy harvested by the entire system at different illuminance values, one can calculate the energy harvested by the system per cm^2 of the solar cell by dividing the total energy by the total size of the solar cell module (that is, 4 cm^2):

At 2 lux, P-SC Avg is 436 nW. Power from 1 cm^2 of harvester is: $109 \text{ nW}/\text{cm}^2$.

At 5 lux, P-SC Avg is 702 nW. Power from 1 cm^2 of harvester is: $175.5 \text{ nW}/\text{cm}^2$.

At 10 lux, P-SC Avg is 1374 nW. Power from 1 cm^2 of harvester is: $343.5 \text{ nW}/\text{cm}^2$.

At 20 lux, P-SC Avg is 2758 nW. Power from 1 cm^2 of harvester is: $689.5 \text{ nW}/\text{cm}^2$.

Considering that at 5 lux, the node requires about 10 min from cold start to harvest enough energy for measuring and transmitting several frames, one can deduce that in such an environment (5 lux), at least six cycles will be possible per hour. Because the capacitor does not fully discharge, and thus harvesting is faster, many more cycles are possible. From Table 6, one can deduce that more than $250 \mu\text{J}$ is harvested at 5 lux in 10 min. From Figure 7, it can be seen that $135 \mu\text{J}$ are needed for a full cycle of the MCU starting up, processing, and transmitting three ADV events. In one hour $6 \times 250 \mu\text{J} = 1500 \mu\text{J}$ will be harvested. This corresponds to about 11 possible activity cycles of the node at 5 lux.

5.6. Limitations

The system behaves as expected. Disconnecting the loads that require the most energy (MCU, touch sensor, and RTC) allows the storage capacitor to be charged at very low illumination levels. The speed at which this process happens depends on the current from the solar cells and hence the illumination. The lower the light level, the longer the delay needed for the storage capacitor voltage to reach the comparator switching threshold. That means approximately 10 min is necessary at 5 lux. Reducing the capacitance of the storage element will lower that time, at the expense of the energy available for the load,

especially for the MCU. In this work, the RSL10 is made to transmit more information than needed. In some cases, it might be enough to transmit less data and less often, depending on the readiness of the receiver. This means that energy could be saved by optimising the communication. This in turn could lead to a longer operational time for the node. There are a certain number of limitations that can be deduced from the measurements.

Input voltage limitation: As the illuminance goes down, so does the maximum voltage that the combination of the four solar cells can reach. This means that for low illuminances, it becomes increasingly difficult to reach the threshold needed for the comparator to trigger and deliver energy to the high consumers. This could be improved by reducing the comparator's threshold. The consequence will be a reduction of the storage's voltage and thus the energy available for the load. One could also add an extra solar cell in series, which also increases the system's cost.

Storage limitation: The leakage of the storage affects the amount of energy lost during harvesting. This will ultimately impact the minimum current required to harvest and store energy. The maximum energy stored in the capacitor and available for the load is also dependant on the storage capacitance. The energy available for the load between storage voltages V_2 and V_1 is: $E = 0.5 \times C \times (V_2^2 - V_1^2)$. The load should be able to work properly between those voltages. For a capacitor of 100 μF , a start voltage of 3 V, and an end voltage of 2 V, the available energy is 250 μJ . Considering that many MEMS (microelectromechanical systems) sensors require only a few microjoules, it can be seen that the system has enough energy to make measurements and transmit the results with a short-range wireless system such as BLE. That energy will not be sufficient for more demanding wireless systems such as LoRa, Sigfox, or WLAN. Another limitation due to the use of a small storage capacitor is the fact that the system switches off quickly if the light level goes beyond 2 lux. This must be taken into account in the use cases.

5.7. Measurements Using Other Light Sources

The spectrum of the light source used influences the amount of energy delivered by a solar cell. This means that for the same illuminance, one can have different energy outputs if the sources used have different spectral components. The type of the solar cell used is also important. Tests were conducted in the light cabinet with fluorescent light. Diffuse light at the window of one office was also used on a cloudy and dark morning to try to catch periods of low illuminance. The tests were conducted at 100 lux because it was not possible to set a lower illuminance for the fluorescent light source in the light cabinet. For diffuse daylight it was not possible to guarantee a steady 100 lux illuminance. These three sources are representative of what is available in several locations that are poorly lit. The results of the measurements are shown in Figure 22. In each case, the upper diagram shows the voltage of the energy storage, and the lower diagram is the illuminance. The voltage of the storage capacitor is measured. It is linked to the energy accumulation in the capacitor and therefore the harvested energy. The capacitor is first discharged (lowest voltage at the beginning of the curves). The system starts harvesting, and the voltage goes up. A first "bump" in the voltage can be seen around 2.2 V because the threshold voltage of the comparator is reached (about 2.2 V). The sensor and RTC are then switched on, leading to a slight decrease in the voltage. The harvesting process continues until the maximum voltage is reached or until the finger sensor is touched, leading to MCU activity. Once the capacitor is discharged below the value allowed by the comparator, the process restarts. It can be seen that the harvesting process is slightly faster with the white LED source than with the fluorescent source (the 2.2 V threshold is reached earlier). With diffuse daylight, the amount of energy harvested is clearly higher. This is not only because of the slight increase in illuminance, but probably also because of the higher irradiance. Successive tests have shown that the behaviours of the system with fluorescent light and with white LED are very close. In all cases, only tens of seconds are needed to harvest enough energy because of the high illuminance values (100 lux). The system works with all the sources.

Lower illuminances will slow down the harvesting but will also work, as seen in the case of the white LEDs.

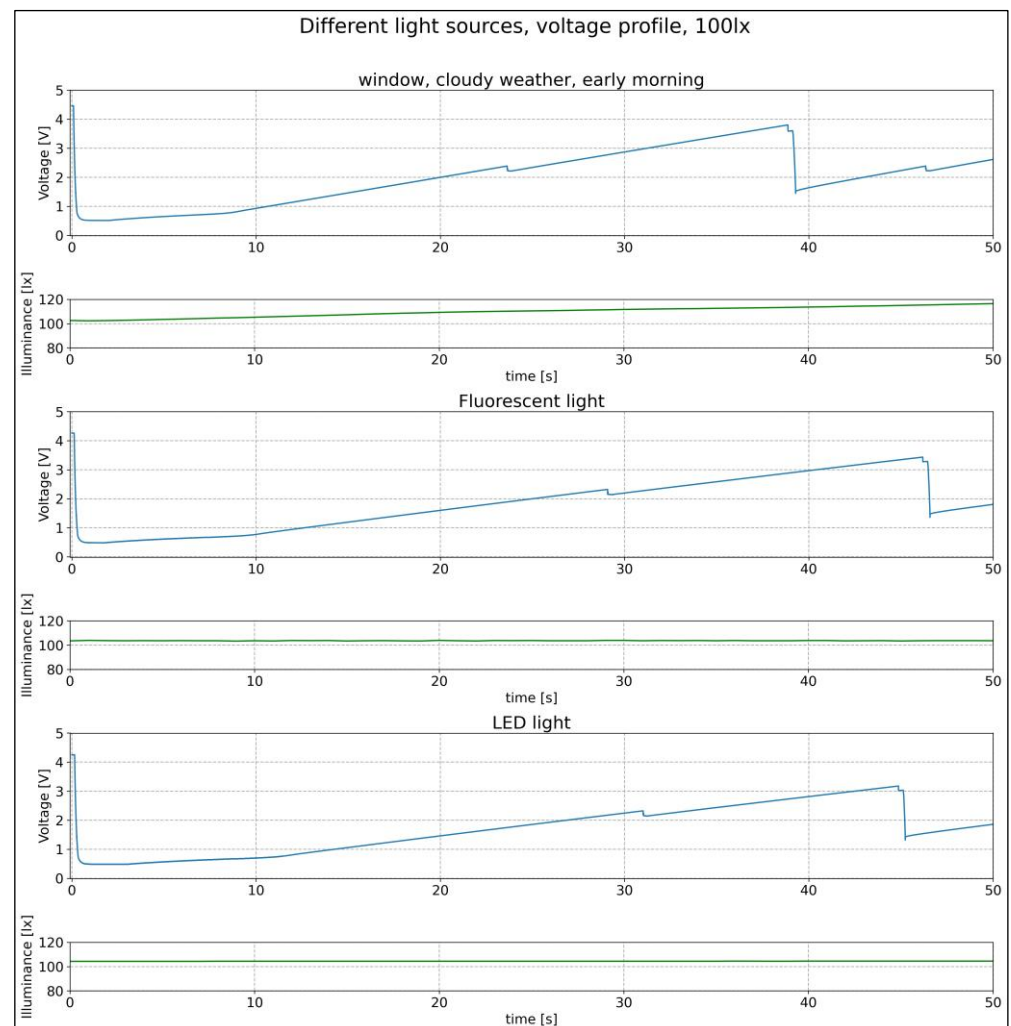


Figure 22. Behaviour of the node at 100 lux for different light sources.

6. Conclusions and Future Works

This work demonstrates an energy-autonomous low-power BLE node, capable of working under illuminances as low as 5 lux. An RTC and a touch sensor are used to switch the main load on or off. This allows the sensing and accurate timing activities to be performed with less than 200 nA. The node can be used in places where it is rather difficult to take advantage of high levels of illuminance in order to save energy. At 5 lux, the system requires less than 10 min to cold-start and measure capacitances. It can also perform some processing and communicate wirelessly (for example, the measurements) using a short-range radio such as BLE. No special storage element is needed, allowing the design to be very simple. The load should fit the amount of energy that is in the storage capacitor. The system can thus take advantage of improvements in the power consumption of processing, sensing, or communication devices. As the illuminance increases, the system can cold-start faster and deal with higher loads (more processing or communication). Although the work here has been performed with a specific solar cell, it can easily be adapted for other solar cells, especially given that issues such as cost, size, longevity, and impact of the solar cell technology on the environment influence the various choices of solar cell technology. The design avoids complex storage elements. Consequently, it reduces costs and sizes and seriously improves the lifetime of the node.

In the near future, it is planned to place all the components on a board in the form and size of a credit card and experiment with different comparator values. The choice of the storage capacitor can then be optimised to further improve the harvesting performances. The system's firmware will be written to control the sensors and implement more functions for sensing and communication. Elements such as FRAM or MRAM (Magnetoresistive Random Access Memory) will also be considered as means of storing data even when the power is off.

Author Contributions: Conceptualization, M.L.M., M.B., P.J.P., M.S. and C.S.K.; methodology, M.L.M. and M.S.; software, S.S.; validation, S.F., B.M. and M.S.; formal analysis, M.L.M. and M.S.; investigation, M.L.M. and M.S.; data curation, M.L.M., S.F. and B.M.; writing—original draft preparation, M.L.M.; writing—review and editing, M.L.M., M.B., P.J.P., M.S. and C.S.K.; visualization, M.L.M., S.F. and B.M.; supervision, M.L.M.; project administration, M.L.M., P.J.P. and C.S.K.; funding acquisition, M.L.M., P.J.P. and C.S.K. All authors have read and agreed to the published version of the manuscript.

Funding: This work was co-funded by the European Union (EU) within the AMANDA project under grant agreement number 825464. The AMANDA project is part of the EU Framework Programme for Research and Innovation Horizon 2020. This work was also co-funded by ZHAW internal projects.

Institutional Review Board Statement: Not applicable.

Informed Consent Statement: Not applicable.

Data Availability Statement: The data are available upon request from the corresponding author.

Conflicts of Interest: P.J. Poole and M. Schellenberg work for Microdul A.G., the firm that designed and produced the touch sensor and the low-voltage comparator. The measurements were, however, carried out by the Zurich University of Applied Sciences. All other authors declare no conflict of interest. The funders had no role in the design of the study; in the collection, analyses, or interpretation of data; in the writing of the manuscript; or in the decision to publish the results.

Appendix A

Illuminance and irradiance in the measurement set up.

Attempts were also made to relate the illuminance values to the irradiance of the light source used. For various values of the illuminance, the irradiance was measured using a pyrometer [70]. The measurements proved difficult at low illuminances. Their interpretation should also take the spectrum of the source into account. The pyranometer used is sensitive and its geometry rather suitable for directed light. It covers a wavelength range from 190 nm to 20,000 nm, making it sensitive to various sources. To minimize the effects of heating sources that could lead to drifts, the light source was switched on and off, and the difference between the measurements (with light on and with light off) was calculated and used as an estimation of the irradiance. The switching was performed manually, respecting the sensor reaction time (given as 1.1 s). Measurements were made with 3 different combinations shown by the 3 curves:

- Glass panel between LEDs and the measurement chamber, reflective walls (blue).
- Glass panel between LEDs and the measurement chamber darkened walls (green).
- No glass panel and darkened walls (orange).

Measurement tables.

The measurement results delivered by the power analyser for Figures 17–20 are shown below. Power and energy values are calculated by the measuring tool.

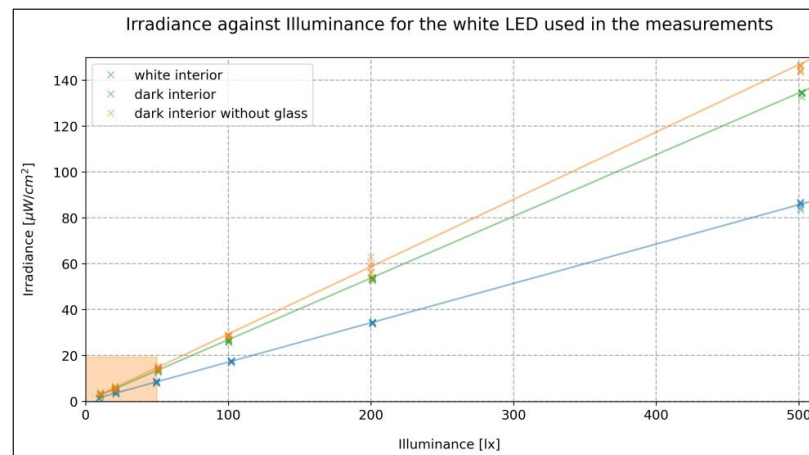


Figure A1. Irradiance measurements against illuminance for the LED source used.

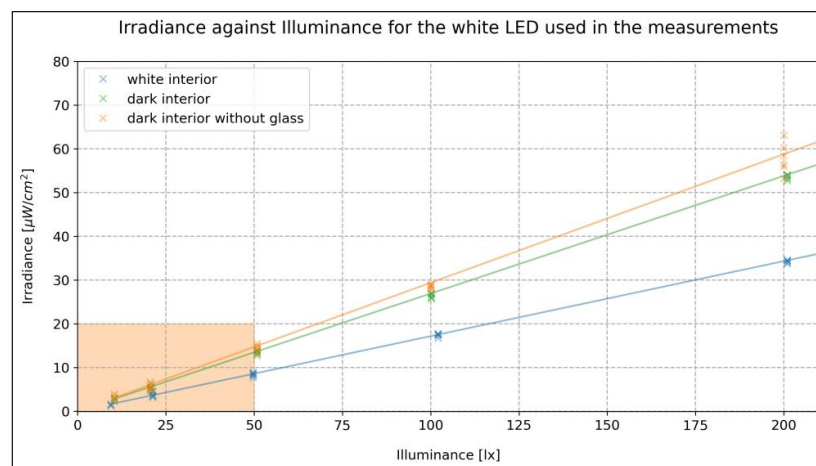


Figure A2. Magnification of small illuminances. Below 50 lux, the measurements are unstable.

Table A1. Relates to Figure 17. Values given by the instrument between the markers for all signals.

Marker 1		Measurements between Markers						Marker 2
Time	04:52.459315	$\Delta = 03:32.127744$						08:24.587059
	Avg	Min	Avg	Max	Peak to Peak	Charge/ Energy	Charge/ Energy	Avg
V-SC	2.132100662 V	2.131851912 V	3.171418731 V	3.713132858 V	1.581280947 V	—	—	3.71262912 V
I-SC	1.708 μ A	266 nA	1.261 μ A	1.958 μ A	1.692 μ A	74 nA h	267.424 μ C	495 nA
P-SC	3.642 μ W	986 nW	3.835 μ W	5.795 μ W	4.809 μ W	226 nW h	813.539 μ J	1.839 μ W
V-MCU	562.646319 mV	449.552357 mV	471.923875 mV	585.626245 mV	136.073887 mV	—	—	470.835164 mV
I-MCU	148 nA	−63 nA	163 nA	315 nA	378 nA	10 nA h	34.665 μ C	161 nA
P-MCU	84 nW	−35 nW	77 nW	148 nW	184 nW	5 nW h	16.358 μ J	76 nW
V-SENS	2.082494775 V	2.079386473 V	3.121259748 V	3.662744045 V	1.583357573 V	—	—	3.662415822 V
I-SENS	157 nA	31 nA	201 nA	11.95 μ A	11.92 μ A	12 nA h	42.573 μ C	168 nA
P-SENS	327 nW	103 nW	631 nW	43.673 μ W	43.57 μ W	37 nW h	133.816 μ J	615 nW

Table A2. Relates to Figure 18. Values given by the instrument between the markers for all signals.

Marker 1		Measurements between Markers						Marker 2
Time	08:25.821594	$\Delta = 390.758 \text{ ms}$ Freq = 2.559 Hz						08:26.212352
	Avg	Min	Avg	Max	Peak to Peak	Charge/ Energy	Charge/ Energy	Avg
V-SC	3.713324308 V	1.889625788 V	3.308414034 V	3.713439226 V	1.823813438 V	—	—	2.083846569 V
I-SC	734 nA	303 nA	1.353 μ A	29.07 μ A	28.767 μ A	147 pA h	529 nC	1.716 μ A
P-SC	2.726 μ W	572 nW	4.423 μ W	107.799 μ W	107.226 μ W	480 pW h	1.728 μ J	3.576 μ W
V-MCU	470.750034 mV	470.456988 mV	3.189349101 V	3.575641632 V	3.105184644 V	—	—	961.210072 mV
I-MCU	192 nA	91 nA	429.744 μ A	17.714757 mA	17.714666 mA	47 nA h	167.926 μ C	141 nA
P-MCU	90 nW	69 nW	1.176826 mW	38.983947 mW	38.983878 mW	128 nW h	459.855 μ J	135 nW
V-SENS	3.470034838 V	2.026766777 V	3.200025449 V	3.471269131 V	1.444502354 V	—	—	2.038153887 V
I-SENS	159 nA	−386 nA	168 nA	9.071 μ A	9.457 μ A	18 pA h	66 nC	189 nA
P-SENS	550 nW	−815 nW	546 nW	31.442 μ W	32.257 μ W	59 pW h	213 nJ	386 nW

Table A3. Relates to Figure 19. Values given by the instrument between the markers for all signals.

Marker 1		Measurements between Markers						Marker 2
Time	337.437 ms	$\Delta = 536.5 \text{ ms}$ Freq = 1.864 Hz						873.938 ms
		Min	Avg	Max	Peak to Peak	Charge/Energy	Charge/Energy	
V-SENS	2.078642607 V	2.067162514 V	2.086894616 V	2.103132963 V	35.970449 mV	—	—	2.097010374 V
I-SENS	843 nA	−1.388 μ A	164 nA	18.71 μ A	20.098 μ A	24 pA h	88 nC	558 nA
P-SENS	1.753 μ W	−2.894 μ W	342 nW	39.035 μ W	41.929 μ W	51 pW h	184 nJ	1.17 μ W
V-MCU	833.948016 mV	600.224555 mV	652.319521 mV	837.72999 mV	237.505436 mV	—	—	603.250086 mV
I-MCU	350 nA	−1.7 μ A	151 nA	1.622 μ A	3.321 μ A	23 pA h	81 nC	52 nA
P-MCU	292 nW	−1.087 μ W	99 nW	1.045 μ W	2.132 μ W	15 pW h	53 nJ	31 nW

Table A4. Relates to Figure 20. Values given by the instrument between the markers for all signals.

Marker 1		Measurements between Markers						Marker 2
Time	−2.624 ms	$\Delta = 234.017 \text{ ms}$ Freq = 4.273 Hz						231.393 ms
		Min	Avg	Max	Peak to Peak	Charge/ Energy	Charge/ Energy	
V-SENS		1.562811852 V	2.081658293 V	2.198033571 V	635.22172 mV	—	—	2.070989132 V
I-SENS		−35.098 μ A	10.4 μ A	92.915 μ A	128.013 μ A	669 pA h	2.407 μ C	169 nA
P-SENS		−76.179 μ W	21.634 μ W	145.209 μ W	221.387 μ W	1 nW h	5.006 μ J	349 nW
V-MCU		980.687022 mV	1.989526746 V	2.197713137 V	1.217026114 V	—	—	2.068371058 V
I-MCU		−8.036295 mA	55.084 μ A	187.327057 mA	195.363352 mA	4 nA h	12.747 μ C	78 nA
P-MCU		−13.461196 mW	101.967 μ W	290.403066 mW	303.864262 mW	7 nW h	23.595 μ J	161 nW

References

1. Market Research on Energy Harvesting for IoT Device. ConFlow Power. 2011. Available online: https://assets.website-files.com/6225ec4d016842cb92d1e5d3/629151680aab9776a55aaad2_Conflow-Energy-Harvesting-Report.pdf (accessed on 28 November 2022).
2. Aileni, R.M.; Suci, G.; Valderrama Sukuyama, C.A.; Pasca, S. Internet of Things and Communication Technology Synergy for Remote Services in Healthcare. In *IoT and ICT for Healthcare Applications*; Gupta, N., Paiva, S., Eds.; EAI/Springer Innovations in Communication and Computing; Springer: Cham, Switzerland; pp. 59–82. [CrossRef]

3. Internet of Things (IoT) Connected Devices Installed Base Worldwide from 2015 to 2025. Statista. Available online: <https://www.statista.com/statistics/471264/iot-number-of-connected-devices-worldwide/> (accessed on 28 November 2022).
4. Komulainen, L.; Ruotsalainen, M. *Billions of IoT Devices in the Field—Huge Negative Impact from Digitalization?* Lappeenranta-Lahti University of Technology: Lahti, Finland, 2022. [CrossRef]
5. Abdul-Qawy, A.S.H. Energy-Harvesting for IoT-based Wireless Nodes: A Progress Study. *J. Soft Comput. Data Min.* **2022**, *3*, 58–67. [CrossRef]
6. Eshaghi, M.; Rashidzadeh, R. An Energy Harvesting Solution for IoT Sensors. In *IEEE International Midwest Symposium on Circuits and Systems (MWSCAS)*; IEEE: New York, NY, USA, 2021; pp. 67–70. [CrossRef]
7. Estrada-López, J.; Abuellil, A.; Zeng, Z.; Sanchez-Sinencio, E. Multiple Input Energy Harvesting Systems for Autonomous IoT End-Nodes. *J. Low Power Electron. Appl.* **2018**, *8*, 6. [CrossRef]
8. Hidalgo-Leon, R.; Urquiza, J.; Silva, C.E.; Silva-Leon, J.; Wu, J.; Singh, P.; Soriano, G. Powering nodes of wireless sensor networks with energy harvesters for intelligent buildings: A review. *Energy Rep.* **2022**, *8*, 3809–3826. [CrossRef]
9. Choudhary, P.; Bhargava, L.; Singh, V.; Choudhary, M.; Suhag, A.K. A survey—Energy harvesting sources and techniques for internet of things devices. *Mater. Today Proc.* **2020**, *30*, 52–56. [CrossRef]
10. Recommended Lighting Levels in Buildings Archtoolbox. Available online: <https://www.archtoolbox.com/recommended-lighting-levels/> (accessed on 28 November 2022).
11. Luxmeter Chauvin Arnoux, CA-1110. Available online: <https://www.chauvin-arnoux.ch/ca-1110.html> (accessed on 28 November 2022).
12. Meli, M.; Hegetschweiler, L. Affordable Energy Autonomous Wireless Sensor for Day and Night. In Proceedings of the Embedded World Conference, Nuremberg, Germany, 23–25 February 2016. [CrossRef]
13. Kouzinopoulos, C.S.; Tzovaras, D.; Bembnowicz, P.; Meli, M.; Bellanger, M.; Kauer, M.; De Vos, J.; Pasero, D.; Schellenberg, M.; Vujicic, O. AMANDA: An Autonomous Self-Powered Miniaturized Smart Sensing Embedded System. In Proceedings of the 2019 IEEE 9th International Conference on Consumer Electronics (ICCE-Berlin), Berlin, Germany, 8–11 September 2019. [CrossRef]
14. Michael, P.R.; Johnston, D.E.; Moreno, W. A Conversion Guide: Solar Irradiance and Lux Illuminance. *J. Meas. Eng.* **2020**, *8*, 153–166. [CrossRef]
15. Charge and Use the SolarCell Remote of Your 2021 Samsung QLED TV. Available online: <https://www.samsung.com/ca/support/tv-audio-video/tv-solarcell-remote/> (accessed on 28 November 2022).
16. Mathews, I.; Kantareddy, S.N.; Buonassisi, T.; Peters, I.M. Technology and Market Perspective for Indoor Photovoltaic Cells. *Joule* **2019**, *3*, 1415–1426. [CrossRef]
17. LEH3—Product Brief. Epishine. Available online: https://4883108.fs1.hubspotusercontent-na1.net/hubfs/4883108/60e2f318bf114d29ba5c714d_LEH3%20Product%20Brief.pdf (accessed on 28 November 2022).
18. Epishine. Indoor Light Energy Harvesting. Available online: <https://www.epishine.com/product> (accessed on 28 November 2022).
19. TDK. Information about the BCS4430B6 BCS Series. Available online: https://product.tdk.com/system/files/dam/doc/product/solar-cell/catalog/film-solarcell_bcs_en.pdf (accessed on 28 November 2022).
20. Lightricity. Datasheet of EXL1-1V20 Solar Cell Module. Available online: <https://lightricity.co.uk/excellight-exl1-1v20> (accessed on 28 November 2022).
21. Juang, S.S.; Lin, P.Y.; Lin, Y.C.; Chen, Y.S.; Shen, P.S.; Guo, Y.L.; Wu, Y.C.; Chen, P. Energy Harvesting Under Dim-Light Condition with Dye-Sensitized and Perovskite Solar Cells. *Front Chem.* **2019**, *7*, 209. [CrossRef] [PubMed]
22. Biswas, S.; Kim, H. Solar Cells for Indoor Applications: Progress and Development. *Polymers* **2020**, *12*, 1338. [CrossRef] [PubMed]
23. Li, B.; Amaratunga, G.A.J. Indoor photovoltaics, the Next Big Trend in solution-processed solar cells. *InfoMat* **2021**, *3*, 445–459. [CrossRef]
24. Mathews, I.; Kelly, G.; King, P.J.; Frizzell, R. GaAs solar cells for Indoor Light Harvesting. In Proceedings of the IEEE 40th Photovoltaic Specialist Conference (PVSC), Denver, CO, USA, 8–13 June 2014. [CrossRef]
25. Lee, H.G.; Chang, N. Powering the IoT: Storage-less and converter-less energy harvesting. In Proceedings of the 20th Asia and South Pacific Design Automation Conference, Chiba, Japan, 19–22 January 2015. [CrossRef]
26. Riaz, A.; Sarker, M.R.; Saad, M.H.M.; Mohamed, R. Review on Comparison of Different Energy Storage Technologies Used in Micro-Energy Harvesting, WSNs, Low-Cost Microelectronic Devices: Challenges and Recommendations. *Sensors* **2021**, *21*, 5041. [CrossRef] [PubMed]
27. Baek, D.; Lee, H.G.; Chang, N. SmartPatch: A Self-Powered and Patchable Cumulative UV Irradiance Meter. *IEEE Des. Test* **2019**, *36*, 57–64. [CrossRef]
28. Meli, M.; Roth, N.; Gutzwiller, P. Wireless sensing using LEDs as very low-cost energy harvesters. In Proceedings of the Embedded World Conference, Nuremberg, Germany, 24–26 February 2015. [CrossRef]
29. Yue, X.; Kauer, M.; Bellanger, M.; Beard, O.; Brownlow, M.; Gibson, D.; Clark, C.; MacGregor, C.; Song, S. Development of an Indoor Photovoltaic Energy Harvesting Module for Autonomous Sensors in Building Air Quality Applications. *IEEE Internet Things J.* **2017**, *4*, 2092–2103. [CrossRef]
30. Wu, F.; Redouté, J.-M.; Yuce, R. A Self-Powered Wearable Body Sensor Network System for Safety Applications. In Proceedings of the 2018 IEEE SENSORS, New Delhi, India, 28–31 October 2018. [CrossRef]
31. Pubill, D.; Serra, J.; Verikoukis, C. Harvesting artificial light indoors to power perpetually a Wireless Sensor Network node. In Proceedings of the 2018 IEEE 23rd International Workshop on Computer Aided Modeling and Design of Communication Links and Networks (CAMAD), Barcelona, Spain, 17–19 September 2018. [CrossRef]

32. Kantareddy, S.N.R.; Mathews, I.; Sun, S.; Layurova, M.; Thapa, J.; Correa-Baena, J.-P.; Bhattacharyya, R.; Buonassisi, T.; Sarma, S.E.; Peters, I.A. Perovskite PV-Powered RFID: Enabling Low-Cost Self-Powered IoT Sensors. *IEEE Sens. J.* **2020**, *20*, 471–478. [CrossRef]
33. Perovskite PV-Powered RFID: Enabling Low-Cost Self-Powered IoT Sensors. Available online: <https://www.youtube.com/watch?v=d6BmzFla6t4> (accessed on 29 November 2022).
34. Michaels, H.; Rinderle, M.; Freitag, R.; Benesperi, I.; Edvinsson, T.; Socher, R.; Gagliardi, A.; Freitag, M. Dye-sensitized solar cells under ambient light powering machine learning: Towards autonomous smart sensors for the internet of things. *Chem. Sci.* **2020**, *11*, 2895–2906. [CrossRef] [PubMed]
35. Rosa, R.L.; Dehollain, C.; Burg, A.; Costanza, M.; Livreri, P. An Energy-Autonomous Wireless Sensor with Simultaneous Energy Harvesting and Ambient Light Sensing. *IEEE Sens. J.* **2021**, *21*, 13744–13752. [CrossRef]
36. Mishu, M.K.; Rokonuzzaman, M.; Pasupuleti, J.; Shakeri, M.; Rahman, K.S.; Binzaid, S.; Tiong, S.K.; Amin, N. An Adaptive TE-PV Hybrid Energy Harvesting System for Self-Powered IoT Sensor Applications. *Sensors* **2021**, *21*, 2604. [CrossRef] [PubMed]
37. Elsys. Sensing Tomorrow. Available online: <https://www.elsys.se/en/> (accessed on 29 November 2022).
38. Meli, M.; Brüttsch, M.; Stajic, S.; Böbel, M.; Lorenz, D.; Hegetschweiler, L.; Karanassos, D.; Kouzinopoulos, C. Low Light Energy Autonomous LoRaWAN Node. In Proceedings of the 2020 IEEE 5th International Symposium on Smart and Wireless Systems within the Conferences on Intelligent Data Acquisition and Advanced Computing Systems (IDAACS-SWS), Dortmund, Germany, 17–18 September 2020. [CrossRef]
39. Vračar, L.; Prijić, A.; Nešić, D.; Dević, S.; Prijić, Z. Photovoltaic Energy Harvesting Wireless Sensor Node for Telemetry Applications Optimized for Low Illumination Levels. *Electronics* **2016**, *5*, 26. [CrossRef]
40. Lin, L.; Jain, S.; Alioto, M. Multi-Sensor Platform with Five-Order-of-Magnitude System Power Adaptation down to 3.1nW and Sustained Operation under Moonlight Harvesting. In Proceedings of the IEEE Symposium on VLSI Circuits, Honolulu, HI, USA, 16–19 June 2020. [CrossRef]
41. Librizzi, F. When to use a standalone RTC IC instead of an MCU embedded RTC in low power IoT devices. Power Electronics News. 2019. Available online: <https://www.powerelectronicsnews.com/when-to-use-a-standalone-rtc-ic-instead-of-an-mcu-embedded-rtc-in-low-power-iot-devices/> (accessed on 12 January 2023).
42. NXP. Datasheet of the PCF2131. Available online: <https://www.nxp.com/docs/en/data-sheet/PCF2131DS.pdf> (accessed on 20 January 2023).
43. Epson. Datasheet of RX-8731LC. Available online: <https://www5.epsondevice.com/en/products/rtc/rx8731lc.html> (accessed on 20 January 2023).
44. Ambiq. Information and Links to Datasheets of RTCs. Available online: <https://ambiq.com/rtc/> (accessed on 20 January 2023).
45. Texas Instruments. Datasheet of TPL5100. Available online: <https://www.ti.com/lit/ds/symlink/tpl5100.pdf> (accessed on 20 January 2023).
46. Microchip. Low Power Touch Design. Available online: <https://ww1.microchip.com/downloads/en/Appnotes/AN2812-Low-Power-Touch-Design-00002812B.pdf> (accessed on 21 January 2023).
47. Renesas. Realizing Low Power Consumption of the Capacitive Touch Sensors with RX140! Available online: <https://www.renesas.com/tw/en/blogs/realizing-low-power-consumption-capacitive-touch-sensors-rx140> (accessed on 21 January 2023).
48. SiLabs. AN507; Low Power Capacitive Sensing. Available online: <https://www.silabs.com/documents/public/application-notes/AN507.pdf> (accessed on 21 January 2023).
49. Hussaini, S.; Jiang, H.; Walsh, P.; MacSweeney, D.; Makinwa, K.A.A. A 15nW Per Button Noise-Immune Readout IC for Capacitive Touch Sensor. In Proceedings of the IEEE 44th European Solid State Circuits Conference (ESSCIRC), Dresden, Germany, 3–6 September 2018. [CrossRef]
50. EM Microelectronic Marin. Datasheet of EM6420 Touch Sensor. Available online: https://www.emmicroelectronic.com/sites/default/files/products/datasheets/em6420_ds.pdf (accessed on 21 January 2023).
51. Aiello, O.; Crovetto, P.; Alioto, M. Wake-Up Oscillators with pW Power Consumption in Dynamic Leakage Suppression Logic. In Proceedings of the IEEE International Symposium on Circuits and Systems (ISCAS), Sapporo, Japan, 26–29 May 2019. [CrossRef]
52. Torrisi, A.; Yıldırım, K.S.; Brunelli, D. Ultra-Low-Power Circuits for Intermittent Communication. *J. Low Power Electron. Appl.* **2022**, *12*, 60. [CrossRef]
53. Epishine. Indoor Light Energy Harvesting (Check for LEH3—Data Sheet). Available online: <https://www.epishine.com/product> (accessed on 29 November 2022).
54. EM Microelectronic Marin. Power Management Controller (Datasheet of the EM8500). Available online: <https://www.emmicroelectronic.com/sites/default/files/products/datasheets/8500-ds.pdf> (accessed on 29 November 2022).
55. E-Peas. Datasheet of AEM10941. Available online: <https://e-peas.com/wp-content/uploads/2022/09/e-peas-AEM10941-datasheet-solar-energy-harvesting.pdf> (accessed on 29 November 2022).
56. Brüttsch, M.; Brülisauer, C.; Widmer, L.; Kräuchi, R.; Truninger, D.; Meli, M. Comparing the energy requirements of bluetooth smart devices. In Proceedings of the Wireless Congress, WEKA, Munich, Germany, 14–15 November 2018. [CrossRef]
57. Lightricity. Outdoor & Space Products (Some Technology Information). Available online: <https://lightricity.co.uk/outdoor-%26-space-products> (accessed on 29 November 2022).
58. Lightricity. Technology. Available online: <https://lightricity.co.uk/technology> (accessed on 21 January 2023).

59. Information About the Comparator is Available from Microdul AG Under Agreement. Available online: <https://ec.europa.eu/research/participants/documents/downloadPublic?documentIds=080166e5ca68bca1&appId=PPGMS> (accessed on 28 November 2022).
60. Micro Crystal. RV-3028-C7 (Main Page for the RTC Module). Available online: <https://www.microcrystal.com/en/products/real-time-clock-rtc-modules/rv-3028-c7/> (accessed on 29 November 2022).
61. Micro Crystal. Datasheet of the RTC Module. Available online: <https://www.microcrystal.com/fileadmin/Media/Products/RTC/Datasheet/RV-3028-C7.pdf> (accessed on 29 November 2022).
62. Micro Crystal. Application Manual RV-3028-C7. Available online: https://www.microcrystal.com/fileadmin/Media/Products/RTC/App.Manual/RV-3028-C7_App-Manual.pdf (accessed on 29 November 2022).
63. Microdul. MS8892B Preliminary Datasheet. Available online: https://www.microdul.com/en/assets/public/images/content/MS8892B_Datasheet_M90-32-0632.pdf (accessed on 29 November 2022).
64. Onsemi. Bluetooth 5.2 Radio System-on-Chip (SoC). Available online: <https://www.onsemi.com/pdf/datasheet/rsl10-d.pdf> (accessed on 29 November 2022).
65. Onsemi. Bluetooth 5.2 System-in-Package (SiP). Available online: <https://www.onsemi.com/pdf/datasheet/rsl10sip-d.pdf> (accessed on 29 November 2022).
66. Onsemi. RSL10-SIP-001GEVB Development Board (User's Manual). Available online: <https://www.onsemi.com/pub/collateral/evbum2565-d.pdf> (accessed on 29 November 2022).
67. Keysight. N6700 Modular Power System Family (Information about N678xA Power Analyser). Available online: <https://www.keysight.com/us/en/assets/7018-05460/data-sheets/5992-1880.pdf> (accessed on 29 November 2022).
68. MAVOLUX 5032 B USB This high Precision Luxmeter (Description of Mavolux 5032B USB Luxmeter). Available online: <https://gossen-photo.de/en/mavolux-5032-b-usb-2/> (accessed on 29 November 2022).
69. Texas Instruments. TIDC-CC2650STK-SENSORTAG (CC2650 SensorTag Used as BLE Sniffer). Available online: <https://www.ti.com/tool/TIDC-CC2650STK-SENSORTAG> (accessed on 29 November 2022).
70. High-Sensitivity Irradiance Measurement Kit. Available online: https://dyenamo.se/analytical_equipment_DN-AE06.php (accessed on 21 January 2023).

Disclaimer/Publisher's Note: The statements, opinions and data contained in all publications are solely those of the individual author(s) and contributor(s) and not of MDPI and/or the editor(s). MDPI and/or the editor(s) disclaim responsibility for any injury to people or property resulting from any ideas, methods, instructions or products referred to in the content.